CHAPTER–2

In Search of Stable, Singlet Metalla *N*-Heterocyclic Carbene (MNHC) and Probing their Potential in Small Molecule Activation.

Abstract: In the first part of this chapter, we have performed density functional theory calculations to design a series of stable, singlet MNHCs. All the MNHCs considered in this study are found to exhibit a stable singlet ground state. The introduction of π-donor groups such as OMe and NMe_2 at the carbene framework significantly increases the ΔE_{S-T} values for the five-membered MNHCs. Furthermore, the calculated ΔE_{S-T} values for some of the MNHCs are found to be significantly large (30–50 kcal mol^{-1}) and lie within the range of the experimentally known carbenes. Therefore, these computationally designed MNHCs – especially those with the ΔE_{S-T} values of more than 40.0 kcal mol^{-1} may be considered as ideal candidates for experimental realization.

In the second part of this chapter, we have performed in-depth computational studies aimed toward probing the efficacy of the MNHCs in activation of small molecules. All the MNHCs have been found to have a stable singlet ground state and exhibit superior electron donating and accepting ability compared to their respective parent carbenes. Furthermore, the calculated energy barrier for the activation of a variety of enthalpically strong bonds for the MNHCs, **1** and **3** are found to be comparable to those obtained for the experimentally evaluated carbenes cyclic(alkyl)(amino)carbene (CAAC) and diamido carbene (DAC), indicating their potential in small molecule activation.

[2.1] In Search of Stable Singlet Metalla-*N*-Heterocyclic Carbenes (MNHCs): A Contribution from Theory

[2.1.1] Introduction

The chemistry of carbenes has evolved as an important area of research over the last couple of decades because of their ease of tunability and versatile catalytic applicability [1–3]. These coordinatively unsaturated compounds can exhibit two different spin states, viz., triplet and singlet. The triplet state arises when both the nonbonding electrons with parallel spin reside in two different mutually perpendicular orbitals, while the singlet spin state results when both the electrons with antiparallel spin occupy the same orbital. Their reactivity is strongly governed by ground state spin multiplicity. For example, the singlet carbene which possesses a filled and available vacant orbital at the central carbon atom can act as an ambiphile, whereas the triplet state can be regarded as a diradical. Even though the parent carbene ($:CH_2$) prefers to have a triplet ground state [4,5], a thorough search of the literature yields a large number of carbenes which favor the singlet state over the triplet state. A signature example of this class of carbene is *N*-heterocyclic carbene (NHC), which was synthesized and isolated by Arduengo et al. in 1991 [6]. The remarkable stability of this class of carbene was attributed to both inductive as well as mesomeric effects imparted by the nitrogen atoms of the carbene ring framework [7]. Many transition metal (TM) complexes have been synthesized bearing NHC as a ligand [8–15] and some of these complexes are being successfully employed in homogeneous catalysis [2,3]. The electron donation ability of the carbene ligand plays a crucial role in determining the catalytic efficiency of the corresponding TM complexes. Therefore, a lot of emphasis has been put towards the design and synthesis of carbenes with better ligand properties and this was generally accomplished by changing either the heteroatom attached to the carbene center or by changing the substituents at the heteroatom as well as by modifying the ring framework itself. For example, the amino group of the carbene ring framework was substituted by other heteroatoms such as phosphorus (PHC) [16,17], oxygen (oxazol-2-ylidene) [18] and sulphur (thiazol-2-ylidene) [18–21]. Other strategies include the alteration of the carbene carbon position (a mesoionic or abnormal carbene) [22–25], considering a saturated backbone instead of an olefinic backbone [26], the expansion of the ring size [27–30], etc. Furthermore, in 2005, Bertrand et al. successfully replaced one of the amino substituents of NHC by an alkyl group and the resultant carbene (popularly

known as CAAC) has significantly enhanced σ-donation as well as π-accepting abilities compared to the conventional NHCs [31,32]. Furthermore, CAAC can also perform reactions like the activation of small molecules such as H_2, CO, P_4, NH_3, etc. [33–35]. Similarly, in 2009, Bielawski et al. reported an intriguing class of carbenes known as diamido carbenes (DACs) that contain two electron-withdrawing carbonyl groups in the carbene backbone. DACs are found to be significantly electrophilic [36] and can carry out reactions like the activation of Si–H bonds in silane [37], N–H bond in NH_3 [38–40], C–H bond insertions [41] etc.

Similarly, attempts have been made to incorporate transition metal (TM) fragments into the carbene ring framework by replacing one of the backbone carbon fragments by isolobal metal fragments (Chart 2.1.1) [42,43]. These types of NHCs containing TM fragments within the carbene ring framework are commonly known as metalla-*N*-heterocyclic carbenes (MNHCs). Interestingly, the computed proton affinity and the pK_a values for the MNHCs are found to be significantly higher than those of traditional NHCs [44], indicating their higher degree of σ-donation ability. Even though MNHCs exhibit better electron donation ability than NHCs, their isolation in the free crystalline state remains an experimental challenge [43]. However, they can be trapped by forming adducts with transition metal complexes such as [AuCl(PPh_3)], [Rh(cod)Cl_2] and CuCl [44].

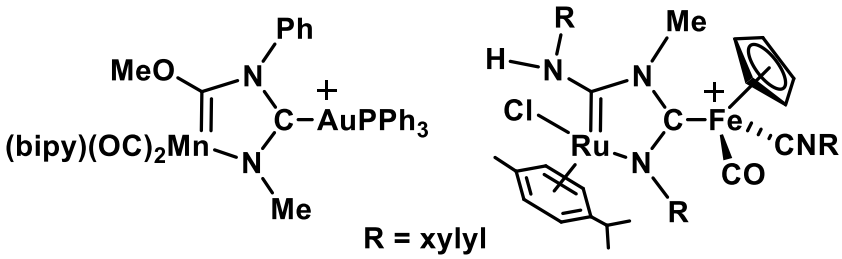

Chart 2.1.1: Experimentally trapped MNHCs by Ruiz *et al* [42, 43].

Although the chemistry of carbenes specifically those of NHCs is well developed, that of MNHCs is still at its infancy. The paucity of a thorough and extensive study on MNHCs may be reasoned to be due to the difficulty associated with its isolation in the free state, which in turn may be attributed to their low singlet–triplet separations [44]. This has prompted us to undertake an in-depth computational study towards the designing of a series of stable singlet MNHCs (Scheme 2.1.1). Herein, we present the results of our computational studies with an intention to build a library of stable five and

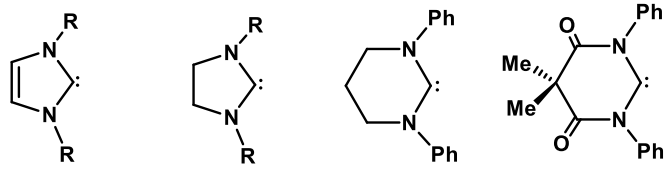

I ; R = CH_3 **II** ; R = CH_3 **III** **IV**
I' ; R = Ph **II'** ; R = Ph

Chart 2.1.2: Types of *N*-heterocyclic carbenes considered in this study.

hitherto unknown six-membered MNHCs by stabilizing their corresponding singlet states. The carbenes illustrated in Chart 2.1.2 are also included for comparison. Although both methyl and phenyl groups were considered to be substituents at the nitrogen atoms of the NHC rings of the five-membered MNHCs, only phenyl groups were considered for six-membered MNHCs, as the parent six-membered NHCs were known only with aryl groups as substituents at the nitrogen atoms.

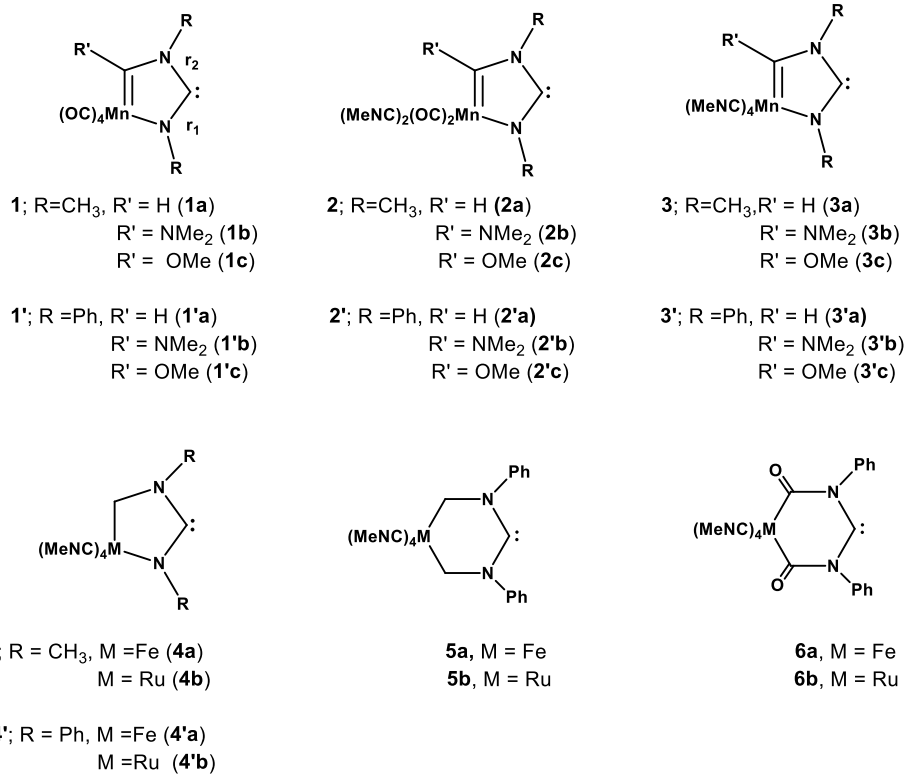

1; R=CH_3, R' = H (**1a**)
R' = NMe_2 (**1b**)
R' = OMe (**1c**)

2; R=CH_3, R' = H **(2a**)
R' = NMe_2 (**2b**)
R' = OMe (**2c**)

3; R=CH_3,R' = H (**3a**)
R' = NMe_2 (**3b**)
R' = OMe (**3c**)

1'; R =Ph, R' = H (**1'a**)
R' = NMe_2 (**1'b**)
R' = OMe (**1'c**)

2'; R =Ph, R' = H (**2'a)**
R' = NMe_2 (**2'b**)
R' = OMe (**2'c**)

3'; R =Ph, R' = H (**3'a)**
R' = NMe_2 (**3'b**)
R' = OMe (**3'c**)

4; R = CH_3, M =Fe (**4a**)
M = Ru (**4b**)

4'; R = Ph, M =Fe (**4'a**)
M =Ru (**4'b**)

5a, M = Fe
5b, M = Ru

6a, M = Fe
6b, M = Ru

Scheme 2.1.1: Schematic representation of the range of MNHCs considered in this study.

[2.1.2] Computational Details

Density functional theory calculations were employed to optimize all the molecules without any geometrical constraints using the hybrid PBE0 exchange–

correlation functional [45,46] in conjunction with the 6-311++G** [47–49] basis set for the main group elements as well as for the first-row transition metals. Furthermore, the relativistic all electron QZP-DKH [50] basis set was considered for heavier transition metal ruthenium with the relativistic second order DKH(DKH2) Hamiltonian [51]. Frequency calculations were carried out at the same level of theory to check the nature of the stationary points and all the structures were characterized as minima with real vibrational frequencies. Bonding analysis was performed with the help of the NBO routine [52,53] as implemented in the Gaussian 09 suit of programs [54]. Furthermore, for calculating the pK_a values for the MNHCs and their corresponding parent carbenes, we have used the thermodynamic cycle as shown in Scheme 2.1.2 [55], where ΔG°gas and ΔG°aq denote the free energy of deprotonation in the gas and aqueous phase, respectively, and $\Delta G°_S$(A) represents the free energy of solvation for species A.

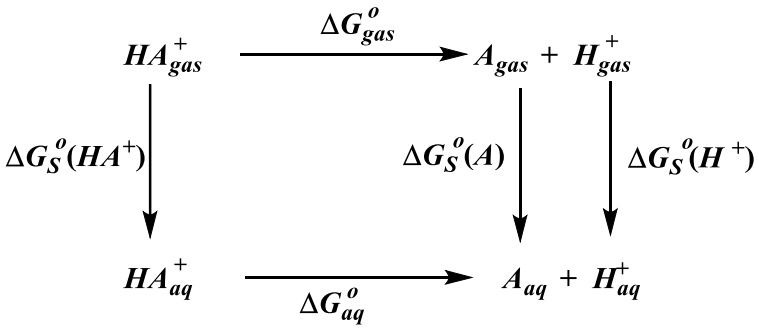

Scheme 2.1.2: Thermodynamic cycle used for the determination of pK_a values.

We know that

$$pK_a = -\log K_a \quad (1)$$

$$\Delta G°_{aq} = -2.303RT\log K_a \quad (2)$$

Therefore, by combining equations (1) and (2), one can determine the pK_a value as

$$pK_a = \Delta G°_{aq} / 2.303RT \quad (3)$$

where the value of $\Delta G°_{aq}$ can be determined from the thermodynamic cycle given in Scheme 2.1.2.

$$\Delta G°_{aq} = G°(A_{aq}) + G°(H^+_{aq}) - G°(HA^+_{aq})$$
$$= G°(A_{gas}) + \Delta G°_S(A) + G°(H^+_{gas}) + \Delta G°_S(H^+)$$
$$- G°(HA^+_{gas}) - \Delta G°_S(HA^+)$$

The standard free energy of solvation, $\Delta G°_S$ (A) for a particular species can be determined by subtracting its gas phase free energy from the solution phase free energy. The solvent effects (H_2O) were estimated by reoptimizing the gas phase optimized

structure using the polarizable continuum model, PCM [56,57]. We have used available values of $G°(H^+_{gas})$ = –6.28 kcal mol^{-1} and $\Delta G°_S$ (H^+) = –265.9 kcal mol^{-1} for our calculations [58-60].

[2.1.3] Results and Discussion

[2.1.3.1] Geometries

The central rings of parent carbenes **I**, **I′** and **II′** have a perfectly planar structure in their optimized singlet state (Figure 2.1.1). However, they get slightly distorted in their corresponding TM fragment incorporated MNHCs. Table 2.1.1 lists the important geometrical parameters for all the molecules considered in this study in their optimized singlet state.

We obtained two separate C_C–N bond lengths (r_1 and r_2, Scheme 2.1.1) for the majority of the MNHCs with r_1 and r_2 being appreciably shorter and longer respectively than the corresponding parent NHCs. The shortening of the r_1 bond may be attributed to the enhanced transfer of electron density from the nitrogen lone pair (LP_N) to the carbenic p_π orbital that is further facilitated by the presence of the electron-rich metal

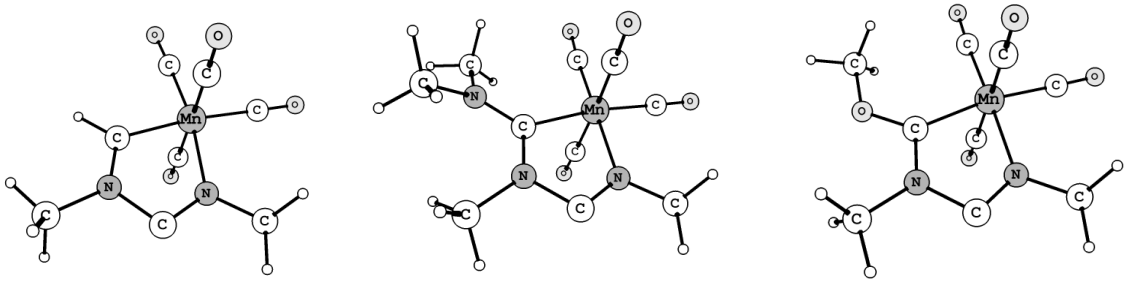

1a **1b** **1c**

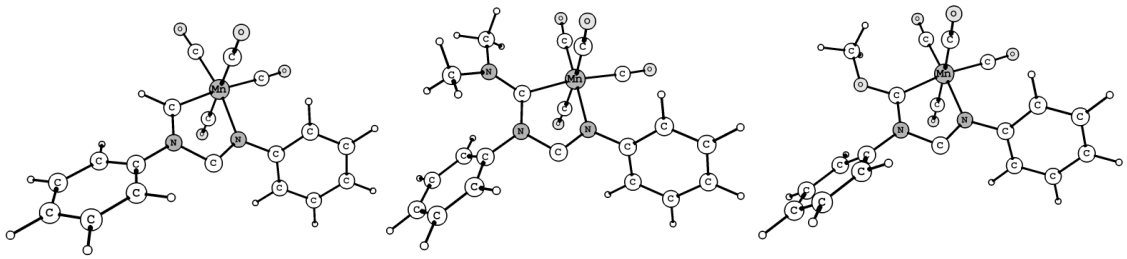

1′a **1′b** **1′c**

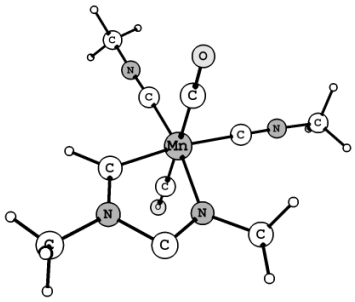

2a

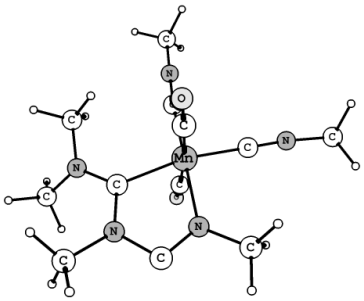

2b

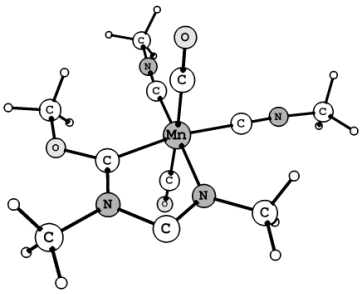

2c

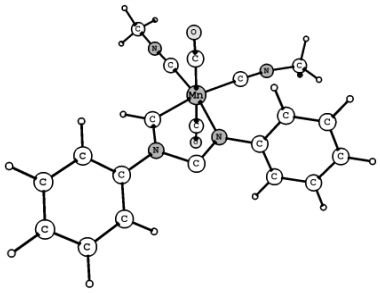

2′a

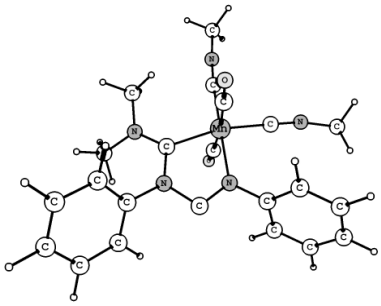

2′b

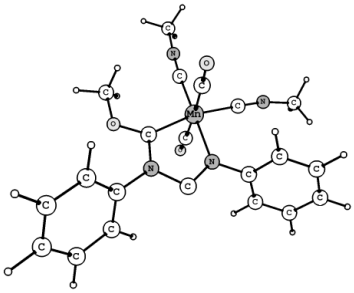

2′c

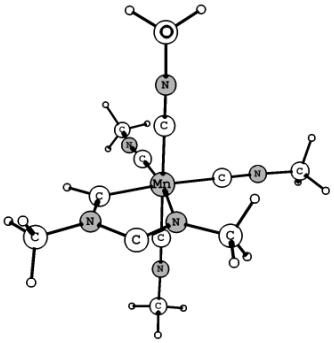

3a

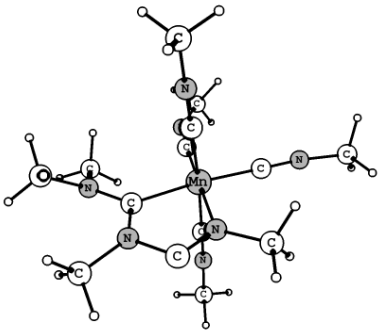

3b

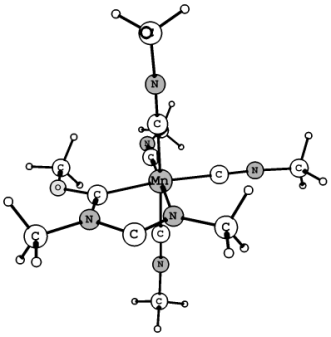

3c

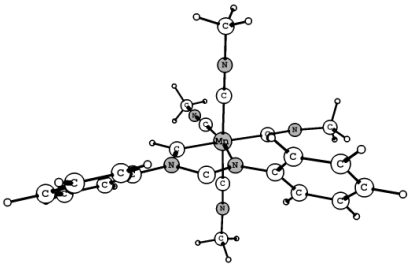

3′a

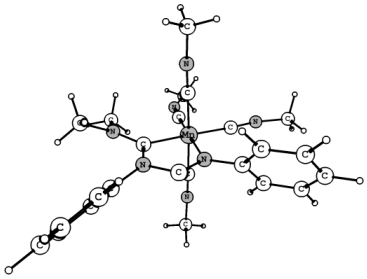

3′b

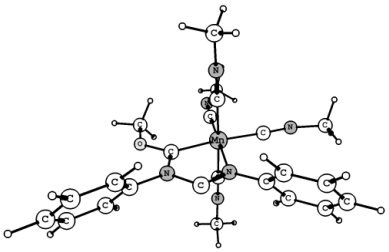

3′c

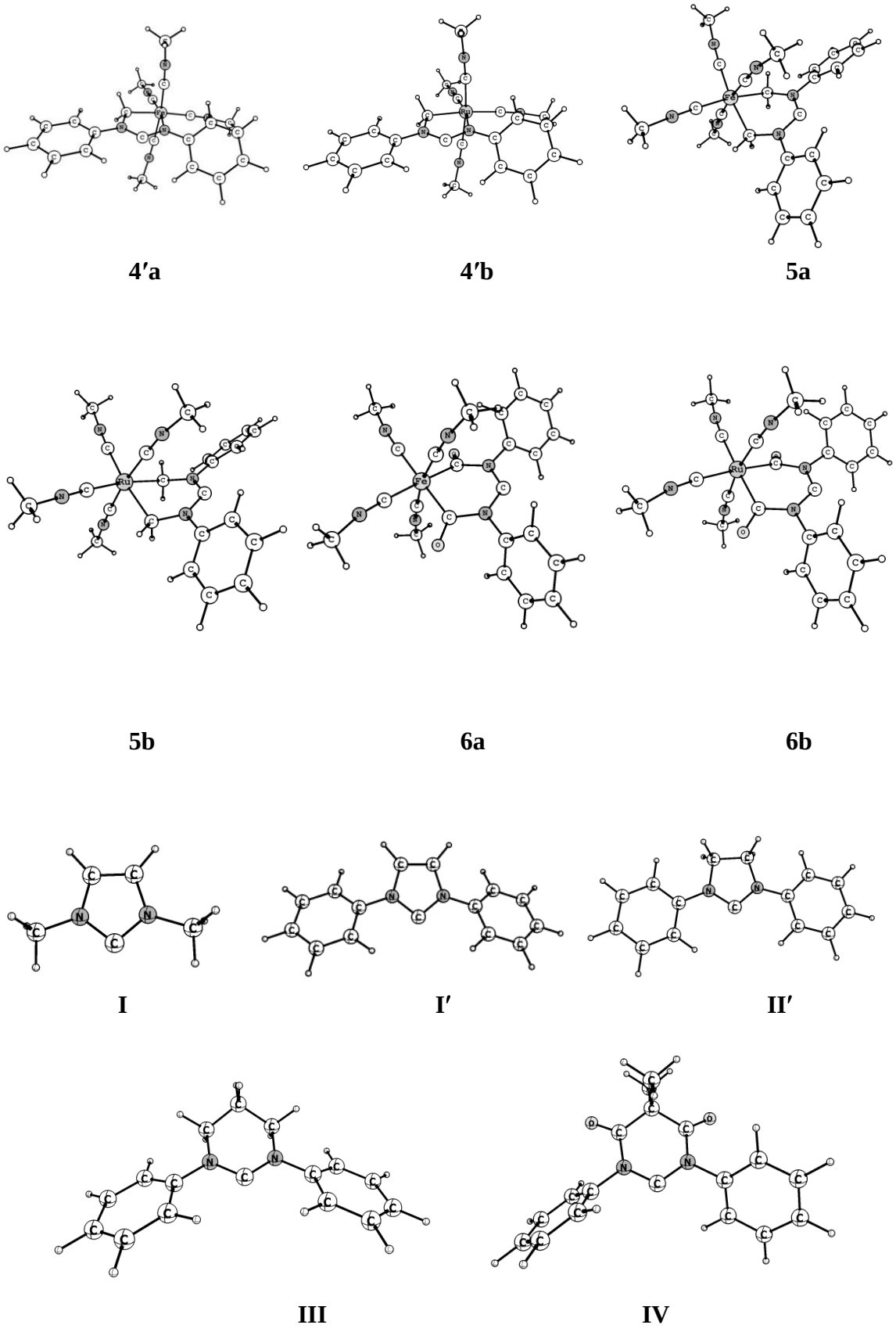

Figure 2.1.1: Singlet state optimized geometries of **1a**–**6b** and **I**–**IV**. (Molecules **4a** and **4b** are excluded)

fragment near the nitrogen atom. The computed geometrical parameters of **1′c** (e.g. r_1 and Mn–N bond lengths, Figure 2.1.2) are found to be in excellent agreement with the experimentally observed values, thereby indicating the reliability of the level of theory used in this study. A comparison of the central ∠N–C_C–N bond angles for MNHCs **1a–4′b** with their respective parent carbenes show that the ∠N–C_C–N bond angle increases significantly from their parent NHCs, which may be attributed to the replacement of smaller carbon atoms by larger metal atoms in MNHCs. Furthermore, **III** and **IV**, which have a distorted geometry in their optimized singlet state, remain distorted even after the

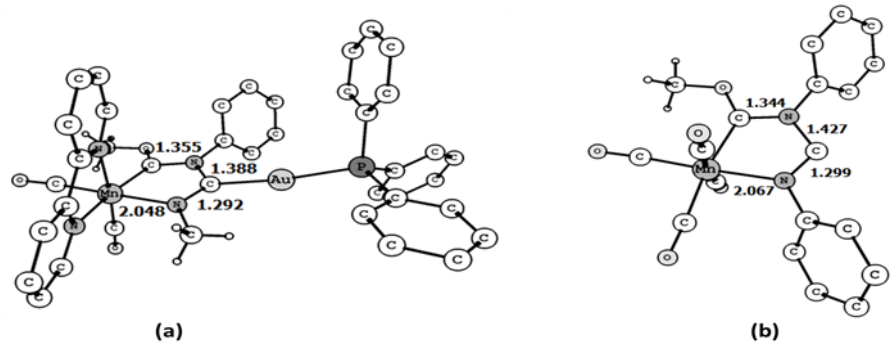

Figure 2.1.2: Figure showing the structure along with key geometrical parameters for the experimentally trapped (**a**) [42] and computationallydesigned MNHC (**b** = **1′c**). (Hydrogen atoms of the phenyl and bipy groups are ommited for the sake of clearity)

incorporation of the TM fragment within the carbene framework. A comparison of the geometrical parameters of **III** with its TM-substituted derivatives **5a–5b** reveals that there is no appreciable change either in the C_C–N bond lengths or in the ∠N–C_C–N bond angle after the installation of the TM fragment into the carbene framework. However, **6a–6b** possess comparable C_C–N bond lengths with parent carbene **IV** but have a slightly wider ∠N–C_C–N angle.

[2.1.3.2] Singlet-Triplet Energy Separations

To the first approximation, the thermodynamic stability of the given carbene molecule may be ascertained in terms of their singlet–triplet separations [61,62]. In general, the higher the singlet–triplet separation (ΔE_{S-T}) of the carbene, the higher the stability of its singlet state. The computed ΔE_{S-T} values of all the MNHCs are given in Table 2.1.2. A careful look at Table 2.1.2 indicates that the ΔE_{S-T} values are effected not only by the substituents at the α-nitrogen atoms and ligands at the TM fragment but also by the substituents present at the carbenic backbone. For molecules **1a–3′c**, the

Table 2.1.1: Computed C_C–N bond lengths (r_1/r_2, in Å), their corresponding Wiberg Bond Index (WBI) values, N–C_C–N bond angles (∠NC_CN in degree) in the singlet state geometry of **1a–6b** and their corresponding parent carbenes.

Molecule	C_C-N(r_1/r_2)	WBI	∠NC_CN	Molecule	C_C-N(r_1/r_2)	WBI	∠NC_CN
I	1.361/1.361	1.249/1.249	102.1	**2′b**	1.299/1.427	1.580/0.970	109.6
I′	1.364/1.364	1.227/1.227	102.1	**2′c**	1.300/1.429	1.585/0.959	108.7
II	1.343/1.343	1.284/1.284	105.8	**3a**	1.295/1.450	1.658/0.924	106.9
II′	1.344/1.344	1.259/1.258	106.1	**3b**	1.293/1.432	1.631/0.962	109.5
III	1.345/1.345	1.271/1.271	116.7	**3c**	1.295/1.431	1.629/0.959	108.7
IV	1.358/1.355	1.210/1.220	116.5	**3′a**	1.303/1.444	1.593/0.938	107.1
1a	1.290/1.457	1.671/0.906	107.3	**3′b**	1.302/1.425	1.570/0.976	109.5
1b	1.291/1.427	1.631/0.968	110.3	**3′c**	1.303/1.427	1.570/0.968	108.7
1c	1.292/1.429	1.634/0.959	109.4	**4a**	1.319/1.349	1.438/1.230	112.3
1′a	1.297/1.456	1.622/0.908	107.4	**4b**	1.321/1.348	1.428/1.238	113.1
1′b	1.298/1.420	1.574/0.981	110.3	**4′a**	1.323/1.359	1.417/1.184	112.3
1′c	1.299/1.427	1.585/0.961	109.5	**4′b**	1.326/1.357	1.402/1.196	113.1
2a	1.293/1.454	1.665/0.914	107.1	**5a**	1.345/1.345	1.268/1.268	117.7
2b	1.292/1.431	1.633/0.961	109.7	**5b**	1.345/1.345	1.272/1.272	118.9
2c	1.293/1.430	1.632/0.956	108.9	**6a**	1.353/1.347	1.234/1.258	120.0
2′a	1.299/1.452	1.615/0.918	106.9	**6b**	1.355/1.347	1.264/1.235	121.1

N-methyl-substituted derivatives yield higher ΔE_{S-T} values than the N-phenyl substituted derivatives. The reduction in the ΔE_{S-T} values of the N-phenylsubstituted derivatives may be attributed to the delocalization of the lone pair at nitrogen (LP_N) to the vacant π* orbitals of the phenyl ring, thereby reducing the extent of electron delocalization from LP_N to C_C [63,64]. On the other hand, introduction of π-donor groups such as – NMe_2 or – OMe at the backbone carbon atom dramatically lifts the ΔE_{S-T} values, i.e., stabilizes the singlet state. Such enhanced stabilization of the singlet state may be attributed to the extensive π-delocalization from the lone pair at the heteroatom of the π-donor group to the carbenic vacant p_π orbital via the p_π orbital of the backbone carbon and the lone pair at nitrogen (alpha to C_C). As a result of this, significant shortening of the C_C–N bonds (r_2) is observed for all the π-donor substituted MNHCs compared to the ones with only hydrogen atoms. For example, the C_C–N bond lengths of **1′b** (1.42 Å) and **1′c** (1.43 Å) are shorter than that for **1′a** (1.46 Å). Similar trends are also observed for **1a–1c** and **2a–3′c**.

Table 2.1.2: Computed singlet-triplet energy separations ($\Delta E_{S\text{-}T}$ in kcal mol^{-1}) of **1a–6b** and their corresponding parent carbenes.

Molecules	$\Delta E_{S\text{-}T}$	Molecules	$\Delta E_{S\text{-}T}$	Molecules	$\Delta E_{S\text{-}T}$
I	80.9	**1′c**	39.0	**3′a**	34.0
I′	68.5	**2a**	34.5	**3′b**	41.4
II′	63.3	**2b**	40.3	**3′c**	43.1
III	51.5	**2c**	45.8	**4′a**	49.2
IV	40.4	**2′a**	31.5	**4′b**	48.0
1a	31.2	**2′b**	40.5	**5a**	38.6
1b	39.3	**2′c**	42.2	**5b**	37.6
1c	43.3	**3a**	37.4	**6a**	36.0
1′a	27.6	**3b**	42.1	**6b**	33.5
1′b	38.1	**3c**	48.0		

As far as the ligands at the TM fragments are concerned, successive or pairwise replacement of the electron withdrawing carbonyl groups (CO) by the strongly donating isonitriles (CNMe) groups gradually increases the singlet state stability. For example, the singlet state stability of **1a–3a** or **1′a–3′a** increases in the order **1a** < **2a** < **3a** and **1′a** < **2′a** < **3′a**. CNMe being a stronger σ-donor but a poorer π-acceptor relative to CO decreases the Lewis acidity of the metal center, thereby facilitating the enhanced transfer of the electron density from the neighboring nitrogen atom to C_C, resulting in higher singlet–triplet separation. This indicates that in order to achieve or stabilize MNHCs in the singlet state, one has to consider an electron-rich transition metal fragment. Accordingly, we have considered only CNMe groups as ligands at the TM center for **4a–6b**. It may be noted that geometry optimizations of the triplet states of **4a–4b** lead to broken geometries, and hence, their ΔE_{S-T} values could not be evaluated. Accordingly, **4a–4b** were not considered for further discussion. Interestingly, the ΔE_{S-T} values of **4′a–6b** are found to be insensitive to the nature of the metal atom.

It can also be seen from Table 2.1.2 and Table 2.1.3 that many of the MNHCs considered in this study have ΔE_{S-T} values that are either comparable or more than that of some of the experimentally known carbenes, indicating that they may be stable enough for experimental realization. To the best of our knowledge, no MNHCs with such large ΔE_{S-T} values (30–50 kcal mol^{-1}) are reported to date and they fall within the range (31.0–85.0 kcal mol^{-1}) of the experimentally known carbenes [65,66].

Table 2.1.3: Calculated ΔE_{S-T} (in kcal mol^{-1}) values for some experimentally known carbenes.

Sl. No.	Molecule	ΔE_{S-T}
1	**CAAC**	38.5
2	**BICAAC**	38.1
3	**6-membered CAAC**	30.8
4	**DAC**	40.4
5	**5-membered DAC**	34.0
6	**aNHC**	48.3

Furthermore, to check the reliability of the calculated ΔE_{S-T} values, we have reoptimized few MNHCs (**1c–3c** and **6a**) as representative cases with a few other functionals. Gratifyingly enough, the ΔE_{S-T} values obtained using these functionals (Table 2.1.4) are comparable to those obtained using PBE0, thereby lending credence to the level of theory used in this study.

Table 2.1.4: Comparison of ΔE_{S-T} values for some representative MNHCs with different functionals.

Molecules	ΔE_{S-T} (kcal mol^{-1})			
	PBE0	**M06**	**ωB97XD**	**TPSSH**
1c	43.3	46.1	46.7	43.4
2c	45.8	48.5	49.3	45.7
3c	48.0	50.1	51.4	47.9
6a	36.0	38.2	41.0	35.1

[2.1.3.3] Ligand Properties

It has been proved by both experimental and theoretical studies that carbenes not only exhibit strong electron donation ability but also possess non-negligible to strong π-accepting ability as well [67–73]. The σ-donation and π-accepting ability of the carbenes can be assessed from an evaluation of the energies of the σ-symmetric donor (E_σ) and π symmetric acceptor (E_π*) molecular orbitals, respectively, centered at C_C. Generally, the higher the energy of the σ symmetric donor orbital, the greater the basicity, while the lower the energy value of the π-symmetric acceptor orbital, the higher the degree of acidity. Similarly, both experimental and theoretical studies have acknowledged the superior electron donation ability of the MNHCs to that of the conventional NHCs

[43,44]. The energies of both the σ- and π-symmetric molecular orbitals for **1a–6b** are listed in Table 2.1.5 and graphically represented as shown in Figure 2.1.3.

It is evident from Table 2.1.5 that for all the five-membered MNHCs **1a–4′b**, there is an increase in the energies of both σ-donor and π-acceptor molecular orbitals as a result of the installation of the TM fragment within the carbene framework from their parent carbenes, implying that the incorporation of the TM fragment leads to an increase and decrease in the σ-donation and π-accepting abilities of the MNHCs, respectively. Therefore, it can be inferred that **1a–4′b** exhibit higher nucleophilic character than that of the corresponding parent carbenes, which is in agreement with previously reported results [42].

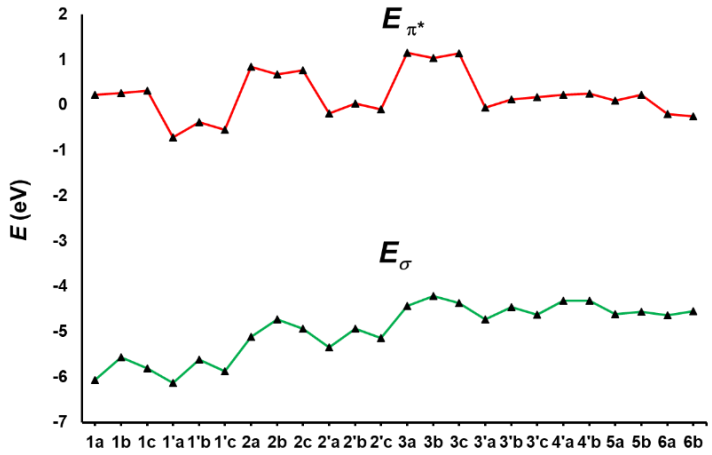

Figure 2.1.3: Plot of the energies of the σ-symmetric lone pair (donor) (E_σ in eV) and π symmetric unoccupied (acceptor) orbitals (E_{π^*} in eV) concentrated on carbene carbon for **1a–6b**.

Furthermore, based on their electron donation ability, MNHCs **1a**, **2a** and **3a** can be arranged in the decreasing order **3a** > **2a** > **1a**. The smallest inductive (−I) effect imparted by the least Lewis acidic TM fragment [Mn(CNMe)$_4$] in **3a** may be reasoned for its superior σ-donation ability compared to **1a** and **2a**. Similarly, based on the calculated energies of the acceptor orbitals (E_π*), these MNHCs may be arranged in the increasing order of π-acidity **3a** < **2a** < **1a**. The reduction in the π-acidity of **3a** compared to that of **1a** may be attributed to the presence of electron-rich and electron-poor TM fragments in **3a** and **1a**, respectively. Therefore, in **3a**, more effective stabilization of the π-symmetric molecular orbital (delocalized over carbene carbon and two nitrogen atoms) takes place, which subsequently increases the energy of the corresponding π-antibonding

Table 2.1.5: Calculated energies of σ-symmertic lone pair orbital (E_σ in eV) and π-symmetric unoccupied orbital (E_{π^*} in eV) centered at carbene carbon, proton affinity (PA in kcal mol^{-1}) , pK_a, pyramidalization angle at the Ga center (θ_{Ga} in degree) and bond dssociation energies of the Ga–C_C bond (BDE, in kcal mol^{-1}) of $GaCl_3$ adducts of **1a–6b** along with their parent carbenes.

Molecules	E_σ	E_{π^*}	PA	pK_a	θ_{Ga}	BDE
I	–6.11	0.62	259.7	21.5	23.5	52.2
I′	–6.42	–0.77	261.7	17.7	24.2	47.3
II′	–6.46	–0.85	256.7	16.3	24.0	40.6
III	–5.84	–0.61	268.5	23.7	30.0	42.4
IV	–6.47	–1.92	252.9	11.8	26.9	35.7
1a	–6.07	0.22	260.7	22.4	26.2	46.8
1b	–5.56	0.27	272.4	27.2	27.7	52.1
1c	–5.81	0.31	267.0	24.1	26.9	47.1
1′a	–6.13	–0.71	265.2	20.1	26.7	44.9
1′b	–5.61	–0.38	276.1	25.2	30.8	46.3
1′c	–5.87	–0.55	272.0	22.2	28.2	46.9
2a	–5.12	0.85	283.0	29.2	29.5	54.9
2b	–4.73	0.67	291.4	32.7	30.3	59.0
2c	–4.93	0.77	287.1	30.4	30.0	54.6
2′a	–5.35	–0.18	283.6	25.9	29.2	51.8
2′b	–4.93	0.03	292.0	30.2	33.2	52.3
2′c	–5.14	–0.09	288.9	28.2	30.8	53.2
3a	–4.43	1.15	299.7	32.7	32.4	63.7
3b	–4.21	1.04	304.9	37.2	31.8	67.2
3c	–4.37	1.14	301.6	34.2	32.7	63.4
3′a	–4.73	–0.06	297.8	31.6	31.5	58.2
3′b	–4.46	0.12	303.3	33.4	34.8	58.0
3′c	–4.62	0.18	301.3	32.5	33.0	59.7
4′a	–4.32	0.22	304.6	34.7	33.4	59.1
4′b	–4.31	0.25	305.3	34.3	34.3	59.0
5a	–4.61	0.10	300.6	33.1	36.8	54.4
5b	–4.56	0.22	301.7	34.4	37.8	54.6
6a	–4.64	–0.20	292.2	26.1	34.6	53.5
6b	–4.55	–0.25	294.0	26.1	35.5	53.6

orbital (E_π*) to a greater extent than that of **1a**, thereby making **3a** a poorer acceptor than **1a**. It is also evident from Table 2.1.5 that N-phenyl substituted MNHCs are better

acceptors than N-methyl substituted MNHCs, while their σ-donation ability is more or less unaffected. On the other hand, the presence of π-donor groups at the carbenic backbone leads to a significant increase in the electron donation ability of these MNHCs. Similarly, for the six-membered MNHCs **5a–5b** and **6a–6b**, there is an increase in the energies of both σ-donor and π-acceptor molecular orbitals as a result of the insertion of the TM fragment within the carbene framework and this makes them better σ-donor ligands but poorer π-acceptor ligands compared to their respective parent carbenes (**III** and **IV**, Table 2.1.5). Among the five- and six-membered MNHCs, **3b** and **6b** are found to have the highest σ-donation ability, respectively.

[2.1.3.4] Proton Affinities

In order to probe the σ-donation ability of the MNHCs, we have calculated their proton affinities (PA) [74]. Typically, the larger the value of PA, the higher the degree of the electron donation ability of the carbene ligand, and interestingly, the calculated PA values of these MNHCs are found to be very high (260–305 kcal mol^{-1}, Table 2.1.5), corroborating their higher degree of nucleophilicity than the parent analogues. We obtained an excellent correlation ($R^2 = 0.95$) between the calculated E_σ and PA values for all the MNHCs (Table 2.1.5 and Figure 2.1.4).

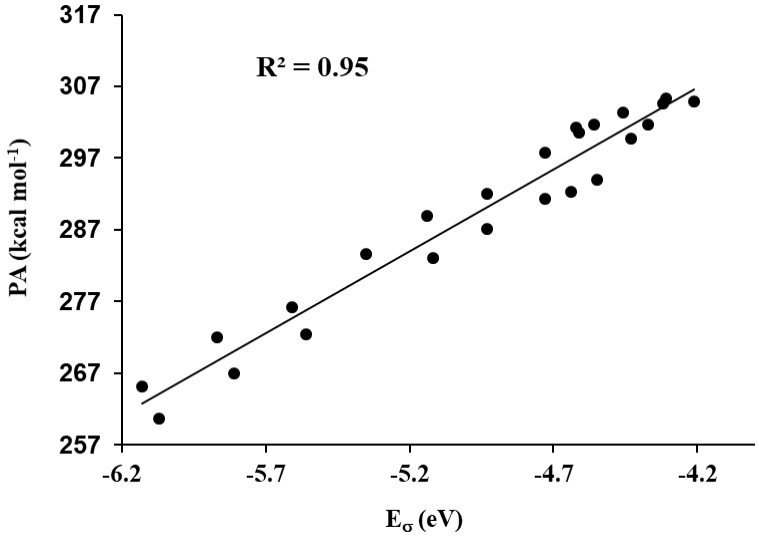

Figure 2.1.4: Correlation plot between the calculated proton affinities (kcal mol^{-1}) and the energies (eV) of σ-symmetric lone pair orbitals concentrated on the carbene carbon for **1a–6b**.

[2.1.3.5] Gallium Pyramidalization

The electron donation ability of the given carbene can be correlated with the degree of pyramidalization at the gallium center (θ_{Ga}; θ_{Ga} = 360 − Σ∠Cl–Ga–Cl) of its adducts with $GaCl_3$ [75]. Accordingly, we have calculated the degree of pyramidalization at the gallium center for the adducts of **1a–6b** with $GaCl_3$ (Table 2.1.5). Generally, the higher the degree of gallium pyramidalization, the higher the degree of the electron donation ability of the carbene ligand under consideration. Indeed, we obtained a reasonable correlation (R^2 = 0.79, omitting the points corresponding to **3b**, **5a** and **5b**) between the calculated θ_{Ga} and E_σ values for all the MNHCs. A good correlation (R^2 = 0.85) is also obtained between the bond dissociation energies of the Ga–C_C bonds with the Ga–C_C bond lengths (Figure 2.1.5).

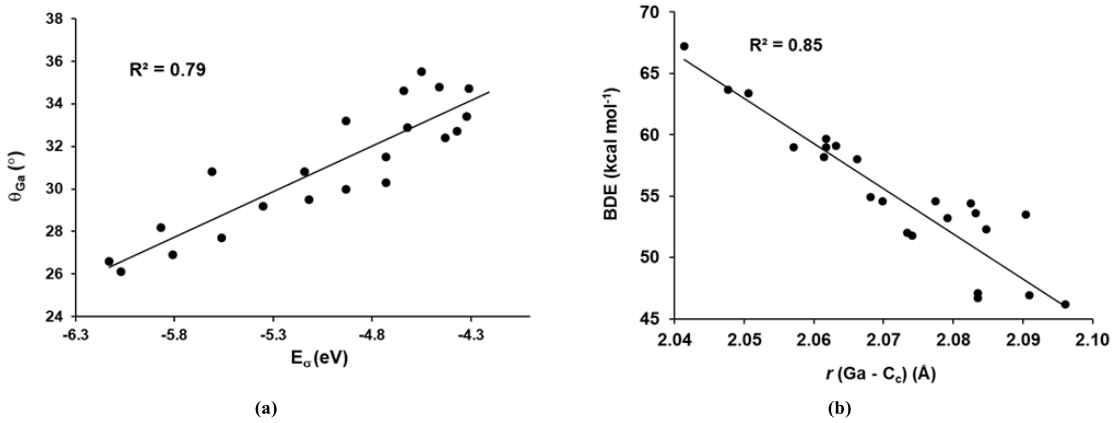

Figure 2.1.5: Correlation plot between (a) pyramidalization angle at the gallium center (θ_{Ga} in degree) of $GaCl_3$ adducts and the energies (eV) of σ-symmetric lone pair orbitals concentrated on the carbene carbon and (b) the bond dissociation energies (kcal mol^{-1}) of Ga–C_C bonds with the Ga–C_C bond lengths (Å) of the $GaCl_3$ adducts of **1a-6b**.

[2.1.3.6] pK_a values

The electron donation ability of these MNHCs was further evaluated using their calculated pK_a values. The calculated pK_a values for the MNHCs lie within the range of 19.0–37.0 (Table 2.1.5), and they are found to be significantly higher compared to their parent carbenes [76,77] implying their higher degree of σ-donation ability, which is in agreement with their respective E_σ values. Indeed, we obtained a good correlation (R^2 = 0.95, omitting the points corresponding to **6a** and **6b**) between the calculated pK_a and E_σ values (Figure 2.1.6).

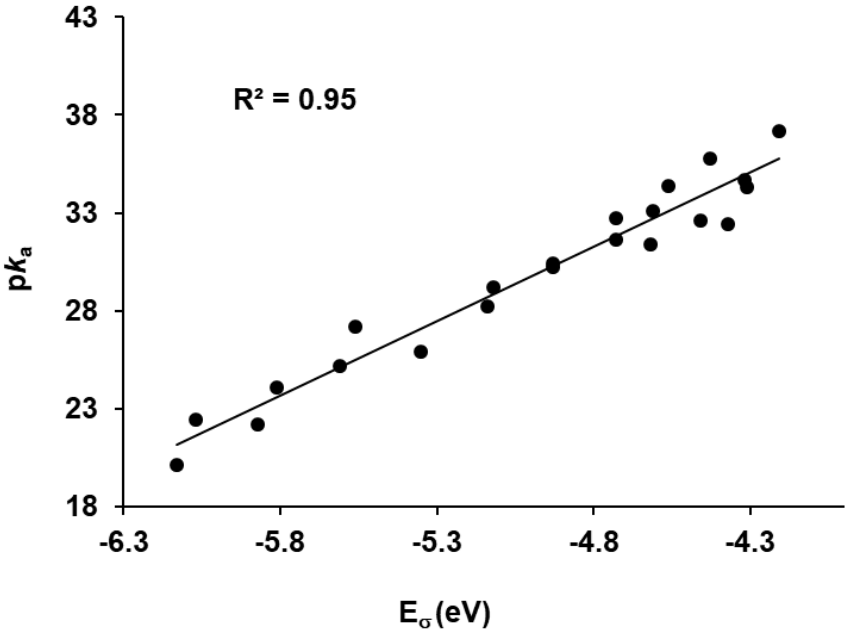

Figure 2.1.6: Correlation plot between pK_a and E_σ (eV) for **1a–6b**.

[2.1.3.7] Nucleophilicity index (*N*)

We have also calculated the nucleophilicity index (*N*) values for all the MNHCs to further assess the σ-donation ability. We have used the equation $N = E_{HOMO} - E_{HOMO(TCNE)}$ to determine the *N* values for the MNHCs by considering tetracyanoethylene (TCNE) as a reference [78]. The calculated *N* values for **1a–6b** along with their parent carbenes are listed in Table 2.1.6. The calculated *N* values for all the MNHCs lie within

Table 2.1.6: Calculated nucleophilicity indices (*N*, in eV) values of **1a–6b** along with their parent analogs.

Molecules	*N*	Molecules	*N*	Molecules	*N*
I	3.6	**1′c**	3.8	**3′a**	5.0
I′	3.3	**2a**	4.6	**3′b**	5.2
II′	3.2	**2b**	5.0	**3′c**	5.1
III	3.9	**2c**	4.8	**4′a**	5.4
IV	3.2	**2′a**	4.4	**4′b**	5.4
1a	3.6	**2′b**	4.8	**5a**	5.1
1b	4.1	**2′c**	4.6	**5b**	5.1
1c	3.9	**3a**	5.3	**6a**	5.1
1′a	3.6	**3b**	5.5	**6b**	5.2
1′b	4.1	**3c**	5.3		

the range of 3.6–5.5 eV and found to be in good agreement with their respective E_σ values. The increased *N* values for all the MNHCs compared to their parent analogues also support their enhanced σ-donation ability compared to those of the conventional NHCs. Among all the MNHCs, **3b** is found to have the highest *N* value, which is in agreement with its E_σ value. Indeed, we obtained a one-to-one correlation between the computed E_σ and *N* values (Figure 2.1.7).

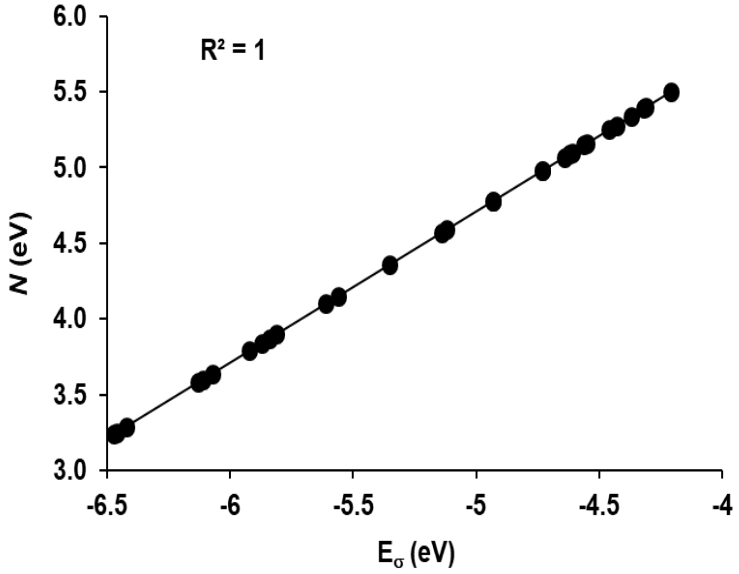

Figure 2.1.7: Correlation plot between *N* (eV) and E_σ (eV) for **1a–6b.**

[2.1.4] Conclusions

Density functional theory calculations have been performed on a series of newly designed MNHCs to stabilize their singlet states. All the MNHCs are found to exhibit a stable singlet ground state. The introduction of π-donor groups such as OMe and NMe_2 at the carbene framework significantly increases the ΔE_{S-T} values for the five-membered MNHCs. Furthermore, the calculated ΔE_{S-T} values for some of the MNHCs are found to be significantly large (30–50 kcal mol^{-1}) and lie within the range of the experimentally known carbenes. Therefore, these computationally designed MNHCs – especially those with the ΔE_{S-T} values of more than 40.0 kcal mol^{-1} may be considered to be ideal candidates for experimental realization. The substituents at the amino groups of the MNHC ring also play a decisive role in determining the ΔE_{S-T} values. MNHCs in which the metal center is attached to strong electron donating ligands such as CNMe results in the significant stabilization of the singlet state indicating that in order to achieve or stabilize MNHCs in the singlet state, one has to consider an electron rich transition metal

fragment. Interestingly, all the MNHCs are found to have better σ-donation ability than their corresponding parent carbenes. The calculated values of PA, pK_a and gallium pyramidalization for the MNHCs are also found to be in good agreement with the σ-donation ability of the MNHCs. We hope that our work will inspire synthetic chemists towards the realization of metalla-*N*-heterocyclic carbenes in the free crystalline state.

[2.1.5] Bibliography

[1] Hopkinson, M. N., Richter, C., Schedler, M., and Glorius, F. An overview of N-heterocyclic carbenes. *Nature*, 510(7506):485-496, 2014.

[2] Nolan, S. P. The Development and Catalytic Uses of N-Heterocyclic Carbene Gold Complexes. *Accounts of Chemical Research*, 44(2):91-100, 2011.

[3] Vougioukalakis, G. C., and Grubbs, R. H. Ruthenium-Based Heterocyclic Carbene-Coordinated Olefin Metathesis Catalysts. *Chemical Reviews*, 110(3):1746-1787, 2010.

[4] Allen, W. D., and Schaefer III, H. F. Geometrical structures, force constants, and vibrational spectra of SiH, SiH_2, SiH_3, and SiH_4. *Chemical Physics*, 108(2):243-274, 1986.

[5] Balasubramanian, K., and McLean, A. D. The singlet–triplet energy separation in silylene. *The Journal of Chemical Physics*, 85(9):5117-5119, 1986.

[6] Arduengo III, A. J., Harlow, R. L., and Kline, M. A Stable Crystalline Carbene. *Journal of the American Chemical Society*, 113(1):361-363, 1991.

[7] Arduengo III, A. J., Dias, H. R., Harlow, R. L., and Kline, M. Electronic Stabilization of Nucleophilic Carbenes. *Journal of the American Chemical Society*, 114(14):5530-5534, 1992.

[8] Dröge, T., and Glorius, F. The Measure of All Rings—N-Heterocyclic Carbenes. *Angewandte Chemie International Edition*, 49(39):6940-6952, 2010.

[9] Frémont, de P., Marion N., and Nolan, S. P. Carbenes: Synthesis, properties, and organometallic chemistry, *Coordination Chemistry Reviews*, 253(7-8):862–892, 2009.

[10] Hahn, F. E., and Jahnke, M. C. Heterocyclic Carbenes: Synthesis and Coordination Chemistry. *Angewandte Chemie International Edition*, 47(17):3122-3172, 2008.

[11] Wanzlick, H. W., and Schönherr, H. J. Direct Synthesis of a Mercury Salt-Carbene Complex. *Angewandte Chemie International Edition in English*, 7(2):141-142, 1968.

[12] Hitchcock, P. B., Lappert M. F., and Pye, P. L. Carbene Complexes. Part 14. The Synthesis and Steric and Electronic Effects in Electron-rich Olefin-derived Bis-, Tris-, and Tetrakis-(Carbene)-ruthenium(II) and a Tetrakis (carbene)osmium(II) Complex; the Crystal and Molecular Structure of *trans*-Dichiorotetrakis(1, 3-diethylimidazo-lidin-2-ylidene)ruthenium(II). *Journal of the Chemical Society, Dalton Transactions,* (7):826–836,1978.

[13] Doyle M. J. and Lappert M. F., Activation Parameters for Rotation about an M–C_{carb} Bond from Temperature Dependent ^{1}H N.m.r. Spectra of Rh^{I} Carbene Complexes. *Journal of the Chemical Society, Chemical Communications*, (17):679–680, 1974.

[14] Lappert, M. F., and Maskell, R. K. Homogeneous catalysis: VIII. Carbene-transition-metal complexes as hydrosilylation catalysts. *Journal of Organometallic Chemistry*, 264(1-2):217-228, 1984.

[15] Öfele, K. 1, 3-Dimethyl-4-imidazolinyliden-(2)-pentacarbonylchrom ein neuer Übergangsmetall-carben-komplex. *Journal of Organometallic Chemistry*, 12(3):P42-P43, 1968.

[16] Martin, D., Baceiredo, A., Gornitzka, H., Schoeller, W. W., and Bertrand, G. A Stable P-Heterocyclic Carbene. *Angewandte Chemie International Edition*, 44(11):1700-1703, 2005.

[17] Masuda, J. D., Martin, D., Lyon-Saunier, C., Baceiredo, A., Gornitzka, H., Donnadieu. B., and Bertrand, G. Stable P-Heterocyclic Carbenes: Scope and Limitations, *Chemistry–An Asian Journal*, 2(1):178-187, 2007.

[18] Ruiz, J., and Perandones, B. F. Metal-induced tautomerization of oxazole and thiazole molecules to heterocyclic carbenes. *Chemical Communications*, (19):2741-2743, 2009.

[19] Vougioukalakis, G. C., and Grubbs, R. H. Synthesis and Activity of Ruthenium Olefin Metathesis Catalysts Coordinated with Thiazol-2-ylidene Ligands. *Journal of the American Chemical Society*, 130(7):2234-2245, 2008.

[20] Raubenheimer, H. G., and Cronje, S. Carbene complexes derived from lithiated heterocycles, mainly azoles, by transmetallation. *Journal of Organometallic Chemistry*, 617-618:170-181, 2001.

[21] Raubenheimer, H. G., Stander, Y., Marais, E. K., Thompson, C., Kruger, G. J., Cronje, S., and Deetlefs, M. Group 6 carbene complexes derived from lithiated azoles and the crystal structure of a molybdenum thiazolinylidene complex. *Journal of Organometallic Chemistry*, 590(2):158-168, 1999.

[22] Gründemann, S., Kovacevic, A., Albrecht, M., Robert, J. W. F., and Crabtree, H. Abnormal binding in a carbene complex formed from an imidazolium salt and a metal hydride complex. *Chemical Communications*, (21):2274-2275, 2001.

[23] Gruendemann, S., Kovacevic, A., Albrecht, M., Faller, J. W., and Crabtree, R. H. Abnormal Ligand Binding and Reversible Ring Hydrogenation in the Reaction of Imidazolium Salts with $IrH_5(PPh_3)_2$. *Journal of the American Chemical Society*, 124(35):10473-10481, 2002.

[24] Mathew, P., Neels, A., and Albrecht, M. 1, 2, 3-Triazolylidenes as Versatile Abnormal Carbene Ligands for Late Transition Metals. *Journal of the American Chemical Society*, 130(41):13534-13535, 2008.

[25] Guisado-Barrios, G., Bouffard, J., Donnadieu, B., and Bertrand, G. Crystalline 1*H*-1, 2, 3-Triazol-5-ylidenes: New Stable Mesoionic Carbenes (MICs). *Angewandte Chemie International Edition*, 49(28):4759-4762, 2010.

[26] Arduengo III, A. J., Goerlich, J. R., and Marshall, W. J. A Stable Diaminocarbene. *Journal of the American Chemical Society*, 117(44):11027-11028, 1995.

[27] Gusev, D. G. Electronic and Steric Parameters of 76 N-Heterocyclic Carbenes in $Ni(CO)_3(NHC)$. *Organometallics*, 28(22):6458-6461, 2009.

[28] Iglesias, M., Beetstra, D. J., Stasch, A., Horton, P. N., Hursthouse, M. B., Coles, S. J., Cavell, K.J., Dervisi, A., and Fallis, I. A. First Examples of Diazepanylidene Carbenes and Their Late-Transition-Metal Complexes. *Organometallics*, 26(19):4800-4809, 2007.

[29] Scarborough, C. C., Guzei, I. A., and Stahl, S. S. Synthesis and isolation of a stable, axially-chiral seven-membered *N*-heterocyclic carbene. *Dalton Transactions*, (13):2284-2286, 2009.

[30] Iglesias, M., Beetstra, D. J., Knight, J. C., Ooi, L. L., Stasch, A., Coles, S., Male, L., Hursthouse, M. B., Cavell, K. J., Dervisi, A. and Fallis, I. A. Novel Expanded Ring N-Heterocyclic Carbenes: Free Carbenes, Silver Complexes, and Structures. *Organometallics*, 27(13):3279-3289, 2008.

[31] Lavallo, V., Canac, Y., Präsang, C., Donnadieu, B., and Bertrand, G. Stable Cyclic (Alkyl)(Amino) Carbenes as Rigid or Flexible, Bulky, Electron-Rich Ligands for Transition-Metal Catalysts: A Quaternary Carbon Atom Makes the Difference. *Angewandte Chemie International Edition*, 44(35): 5705-5709, 2005.

[32] Lavallo, V., Canac, Y., DeHope, A., Donnadieu, B., and Bertrand, G. A Rigid Cyclic (Alkyl)(amino) carbene Ligand Leads to Isolation of Low-Coordinate Transition-Metal Complexes. *Angewandte Chemie International Edition*, 44(44):7236-7239, 2005.

[33] Frey, G. D., Lavallo, V., Donnadieu, B., Schoeller, W. W., and Bertrand, G. Facile Splitting of Hydrogen and Ammonia by Nucleophilic Activation at a Single Carbon Center. *Science*, 316(5823):439-441, 2007.

[34] Lavallo, V., Canac, Y., Donnadieu, B., Schoeller, W. W., and Bertrand, G. CO Fixation to Stable Acyclic and Cyclic Alkyl Amino Carbenes: Stable Amino Ketenes with a Small HOMO–LUMO Gap. *Angewandte Chemie International Edition*, 45(21):3488-3491, 2006.

[35] Masuda, J. D., Schoeller, W. W., Donnadieu, B., and Bertrand, G. Carbene Activation of P_4 and Subsequent Derivatization. *Angewandte Chemie International Edition*, 46(37):7052-7055, 2007.

[36] Hudnall, T. W., and Bielawski, C. W. An *N*, *N*′-Diamidocarbene: Studies in C−H Insertion, Reversible Carbonylation, and Transition-Metal Coordination Chemistry. *Journal of the American Chemical Society*, 131(44):16039-16041, 2009.

[37] Lastovickova, D. N., Moerdyk, J. P., Kelley, A. R., and Bielawski, C. W. Assessing the reactivity of the *N*, *N*′-diamidocarbenes toward compounds containing early p-block elements. *Journal of Physical Organic Chemistry*, 28(2):75-78, 2015.

[38] Hudnall, T. W., Moerdyk, J. P., and Bielawski, C. W. Ammonia N–H activation by a *N*, *N*′-diamidocarbene. *Chemical Communications*, 46(24):4288-4290, 2010.

[39] Moerdyk, J. P., and Bielawski, C. W. Reductive generation of stable, five-membered *N*, *N*′-diamidocarbenes. *Chemical Communications*, 50(35):4551-4553, 2014.

[40] Moerdyk, J. P., Blake, G. A., Chase, D. T., and Bielawski, C. W. Elucidation of Carbene Ambiphilicity Leading to the Discovery of Reversible Ammonia Activation. *Journal of the American Chemical Society*, 135(50):18798-18801, 2013.

[41] Moerdyk, J. P., and Bielawski, C. W. *N*, *N*′-Diamidocarbenes Facilitate Selective C–H Insertions and Transfer Hydrogenations. *Chemistry–A European Journal*, 19(44):14773-14776, 2013.

[42] Ruiz, J., García, L., Perandones, B. F., and Vivanco, M. A Fischer carbene within an Arduengo carbene. *Angewandte Chemie International Edition*, 50(13):3010-3012, 2011.

[43] Ruiz, J., García, L., Mejuto, C., Vivanco, M., Díaz, M. R., and García-Granda, S. Strong electron-donating metalla-N-heterocyclic carbenes. *Chemical Communications*, 50(17):2129-2132, 2014.

[44] Ruiz, J., García, L., Vivanco, M., Berros, Á., and Van der Maelen, J. F. Generating and Trapping Metalla-N-Heterocyclic Carbenes. *Angewandte Chemie International Edition*, 54(14):4212-4216, 2015.

[45] Ernzerhof, M., and Scuseria, G. E. Assessment of the Perdew–Burke–Ernzerhof exchange-correlation functional. *The Journal of Chemical Physics*, 110(11):5029-5036, 1999.

[46] Adamo, C., and Barone, V. Toward reliable density functional methods without adjustable parameters: The PBE0 model. *The Journal of Chemical Physics*, 110(13):6158-6170, 1999.

[47] Francl, M. M., Pietro, W. J., Hehre, W. J., Binkley, J. S., Gordon, M. S., DeFrees, D. J., and Pople, J. A. Self-consistent molecular orbital methods. XXIII. A polarization-type basis set for second-row elements. *The Journal of Chemical Physics*, 77(7):3654-3665, 1982.

[48] Rassolov, V. A., Pople, J. A., Ratner, M. A., and Windus, T. L. 6-31G* basis set for atoms K through Zn. *The Journal of Chemical Physics*, 109(4):1223-1229, 1998.

[49] Rassolov, V. A., Ratner, M. A., Pople, J. A., Redfern, P. C., and Curtiss, L. A. 6-31G* basis set for third-row atoms. *Journal of Computational Chemistry*, 22(9):976-984, 2001.

[50] Ceolin, G. A., de Berrêdo, R. C., and Jorge, F. E. Gaussian basis sets of quadruple zeta quality for potassium through xenon: application in CCSD (T) atomic and molecular property calculations. *Theoretical Chemistry Accounts*, 132:1339, 2013.

[51] Jansen, G., and Hess, B. A. Revision of the Douglas-Kroll transformation. *Physical Review A*, 39(11):6016, 1989.

[52] Glendening, E. D., Reed, A. E., Carpenter, J. E., and Weinhold, F. NBO Program, version 3.1; University of Wisconsin: Madison, WI, 1988

[53] Reed, A. E., Curtiss, L. A., and Weinhold, F. Intermolecular Interactions from a Natural Bond Orbital, Donor-Acceptor Viewpoint. *Chemical Reviews*, 88(6):899-926, 1988.

[54] Frisch, M. J., Trucks, G. W., Schlegel, H. B., Scuseria, G. E., Robb, M. A., Cheeseman, J. R., Montgomery, J. A., Jr., Vreven, T., Kudin, K. N., Burant, J. C., Millam, J. M., Iyengar, S. S., Tomasi, J., Barone, V., Mennucci, B., Cossi, M., Scalmani, G., Rega, N., Petersson, G. A., Nakatsuji, H., Hada, M., Ehara, M., Toyota, K., Fukuda, R., Hasegawa, J., Ishida, M., Nakajima, T., Honda, Y., Kitao, O., Nakai, H., Klene, M., Li, X., Knox, J. E., Hratchian, H. P., Cross, J. B., Bakken, V., Adamo, C., Jaramillo, J., Gomperts, R., Stratmann, R. E., Yazyev, O., Austin, A. J., Cammi, R., Pomelli, C., Ochterski, J. W., Ayala, P. Y., Morokuma, K., Voth, G. A., Salvador, P. J., Dannenberg, J., Zakrzewski, V. G., Dapprich, S., Daniels, A. D., Strain, M. C., Farkas, O., Malick, D. K., Rabuck, A. D., Raghavachari, K., Foresman, J. B., Ortiz, J. V., Cui, Q., Baboul, A. G., Clifford, S., Cioslowski, J., Stefanov, B. B., Liu, G., Liashenko, A., Piskorz, P., Komaromi, I., Martin, R. L., Fox, D. J., Keith, T., Al- Laham, M. A., Peng, C. Y., Nanayakkara, A., Challacombe, M., Gill, P. M. W., Johnson, B., Chen, W., Wong, M. W., Gonzalez, C., and Pople, J. A. *Gaussian 03*, *Revision D.02*; Gaussian, Inc., Pittsburgh, PA, 2003.

[55] Magill, A. M., Cavell, K. J., and Yates, B. F. Basicity of Nucleophilic Carbenes in Aqueous and Nonaqueous Solvents Theoretical Predictions. *Journal of the American Chemical Society*, 126(28):8717-8724, 2004.

[56] Cossi, M., Scalmani, G., Rega, N., and Barone, V. New developments in the polarizable continuum model for quantum mechanical and classical calculations on molecules in solution. *The Journal of Chemical Physics*, 117(1):43-54, 2002.

[57] Tomasi, J., and Persico, M. Molecular Interactions in Solution: an Overview of Methods Based on Continuous Distributions of the Solvent. *Chemical Reviews*, 94(7):2027-2094, 1994.

[58] Camaioni, D. M., and Schwerdtfeger, C. A. Comment on "Accurate Experimental Values for the Free Energies of Hydration of H^+, OH^-, and H_3O^+". *The Journal of Physical Chemistry A*, 109(47):10795-10797, 2005.

[59] Ho, J., and Coote, M. L. A universal approach for continuum solvent pK_a calculations: are we there yet?. *Theoretical Chemistry Accounts*, 125(1):3-21, 2010.

[60] Liptak, M. D., and Shields, G. C. Accurate pK_a Calculations for Carboxylic Acids Using Complete Basis set and Gaussian-n Models Combined with CPCM Continuum Solvation Methods. *Journal of the American Chemical Society*, 123(30):7314-7319, 2001.

[61] Bourissou, D., Guerret, O., Gabbaï, F. P., and Bertrand, G. Stable Carbenes. *Chemical Reviews*, 100(1):39-92, 2000.

[62] Gronert, S., Keeffe, J. R., and More O'Ferrall, R. A. Stabilities of Carbenes: Independent Measures for Singlets and Triplets. *Journal of the American Chemical Society*, 133(10):3381-3389, 2011.

[63] Munz, D. Pushing Electrons– Which Carbene Ligand for Which Application?. *Organometallics*, 37(3):275-289, 2018.

[64] Martin, D., Lassauque, N., Donnadieu, B., and Bertrand, G. A Cyclic Diaminocarbene with a Pyramidalized Nitrogen Atom: A Stable N-Heterocyclic Carbene with Enhanced Electrophilicity. *Angewandte Chemie International Edition*, 51(25):6172-6175, 2012.

[65] Melaimi, M., Soleilhavoup, M., and Bertrand, G. Stable Cyclic Carbenes and Related Species Beyond Diaminocarbenes. *Angewandte Chemie International Edition*, 49(47):8810-8849, 2010.

[66] Weinstein, C. M., Junor, G. P., Tolentino, D. R., Jazzar, R., Melaimi, M., and Bertrand, G. Highly Ambiphilic Room Temperature Stable Six-Membered Cyclic (Alkyl)(amino) carbenes. *Journal of the American Chemical Society*, 140(29):9255-9260, 2018.

[67] Boehme, C., and Frenking, G. Electronic Structure of Stable Carbenes, Silylenes, and Germylenes. *Journal of the American Chemical Society*, 118(8):2039-2046, 1996.

[68] Tukov, A. A., Normand, A. T., and Nechaev, M. S. *N*-heterocyclic carbenes bearing two, one and no nitrogen atoms at the ylidene carbon: insight from theoretical calculations. *Dalton Transactions*, (35):7015-7028, 2009.

[69] Bazinet, P., Yap, G. P., and Richeson, D. S. Constructing a Stable Carbene with a Novel Topology and Electronic Framework. *Journal of the American Chemical Society*, 125(44):13314-13315, 2003.

[70] Nair, V., Bindu, S., and Sreekumar, V. N-Heterocyclic Carbenes: Reagents, Not Just Ligands!. *Angewandte Chemie International Edition*, 43(39):5130-5135, 2004.

[71] Phukan, A. K., Guha, A. K., Sarmah, S., and Dewhurst, R. D. Electronic and Ligand Properties of Annelated Normal and Abnormal (Mesoionic) *N*-heterocyclic Carbenes: A Theoretical Study. *The Journal of Organic Chemistry*, 78(21):11032-11039, 2013.

[72] Borthakur, B., Rahman, T., and Phukan, A. K. Tuning the Electronic and Ligand Properties of Remote Carbenes: A Theoretical Study. *The Journal of Organic Chemistry*, 79(22):10801-10810, 2014.

[73] Guha, A. K., and Phukan, A. K. Theoretical Study on the Effect of Annelation and Carbonylation on the Electronic and Ligand Properties of *N*-Heterocyclic Silylenes and Germylenes: Carbene Comparisons begin To Break Down. *The Journal of Organic Chemistry*, 79(9):3830-3837, 2014.

[74] Tonner, R., Heydenrych, G., and Frenking, G. First and Second Proton Affinities of Carbon Bases. *ChemPhysChem*, 9(10):1474-1481, 2008.

[75] El-Hellani, A., Monot, J., Tang, S., Guillot, R., Bour, C., and Gandon, V. Relationship between Gallium Pyramidalization in L·$GaCl_3$ Complexes and the Electronic Ligand Properties. *Inorganic Chemistry*, 52(19):11493-11502, 2013.

[76] Magill, A. M., and Yates, B. F. An Assessment of Theoretical Protocols for Calculation of the pK_a Values of the Prototype Imidazolium Cation. *Australian Journal of Chemistry*, 57(12):1205-1210, 2004.

[77] Alder, R. W., Allen, P. R., and Williams, S. J. Stable Carbenes as Strong Bases. *Journal of the Chemical Society, Chemical Communications*, (12):1267-1268, 1995.

[78] Domingo, L. R., Chamorro, E., and Pérez, P. Understanding the Reactivity of Captodative Ethylenes in Polar Cycloaddition Reactions. A Theoretical Study. *The Journal of Organic Chemistry*, 73(12):4615-4624, 2008.

[2.2] Probing the Potential of Metalla-*N*-Heterocyclic Carbenes Towards Activation of Enthalpically Strong Bonds

[2.2.1] Introduction

Historically, carbenes were thought to be reactive species and reaction intermediates that played important roles in several organic transformations [1]. With the isolation of a stable singlet acyclic carbene by Bertrand and co-workers [2] as well as the first crystalline *N*-heterocyclic carbene (NHC) by Arduengo and coworkers [3], carbene chemistry experienced rapid development over the ensuing decades [4–9]. The fascinating electronic properties of NHCs, including their tunable electron donor and acceptor abilities, make them an important class of ligands in various transition metal (TM)-based, and TM-free transformations [10–14]. Various efforts have been made to modify the electronic properties of NHCs, which include variation of the N-bound flanking substituent, substitution of the amino groups and backbone carbon atoms of the NHC ring by other heteroatoms [15–28] and variation of carbene carbon position with respect to the heteroatoms etc. [29–32]. Similarly, efforts have also been made to substitute the carbene carbon of the NHC framework by other heteroatoms such as phosphorous and silicon etc. [33–37]. In 2005, Bertrand and coworkers successfully replaced one of the amino groups of the NHC ring by a saturated carbon center, thereby generating a new class of carbenes commonly known as cyclic alkyl(amino)carbenes (CAACs) [38,39]. Interestingly, CAACs possess significantly enhanced σ-donor properties and π-acidity when compared to the conventional imidazol-2-ylidenes and are capable of activating small molecules [40–42] and enthalpically robust bonds, such as P–H, B–H, Si–H, C–F and C–H etc. [43–47]. In addition, CAACs are being extensively used for the stabilization of highly reactive main group element compounds as well as low valent TM complexes which are widely used in organocatalyst [7,8,48–50]. In 2009, Bielawski and coworkers reported the isolation of another intriguing class of carbenes known as diamidocarbenes (DACs) [51] which also possess significant electrophilic character and can activate enthalpically strong E–H (E = N, P, Si) bonds [52–57]. Furthermore, in a seminal study, Ruiz and coworkers reported the synthesis of a novel class of NHC that incorporates a TM fragment within the carbene framework [58]. These type of NHCs bearing TM fragments within the carbene ring framework are commonly known as metalla-*N*-heterocyclic carbenes (MNHCs). Interestingly, the calculated pK_a and proton affinity values for the MNHCs were found to be significantly higher than that

of the conventional imidazol-2-ylidenes implying their higher degree of nucleophilicity [59]. Although MNHCs exhibit enhanced electronic properties when compared to conventional NHCs, their isolation in the free crystalline state has remained a difficult experimental challenge for the synthetic chemist [58]. In this context, it is worth mentioning the recent discovery of a four membered metallacycle bearing a free carbene by Tonks and co-workers [60].

Although the literature is rich with stability and reactivity studies related to NHCs [61–66], only a few reports have considered MNHCs. In this context, it is worth mentioning the very recent seminal discovery of a stable *N*-hetero-metallacyclic silylene – the first cyclic silylene known till date to activate H_2 at room temperature [67]. In the first part of this chapter, we have proposed a series of MNHCs that were determined computationally to have significantly greater stabilities as ascertained from their calculated singlet–triplet energy separation values. Herein, we present the results of further study aimed towards probing the efficacy of these MNHCs in activation of small molecules (Scheme 2.2.1). For the sake of comparison, we have also included the experimentally evaluated ambiphilic carbenes DAC (**III**) and CAAC (**IV**) in our study (Figure 2.2.1).

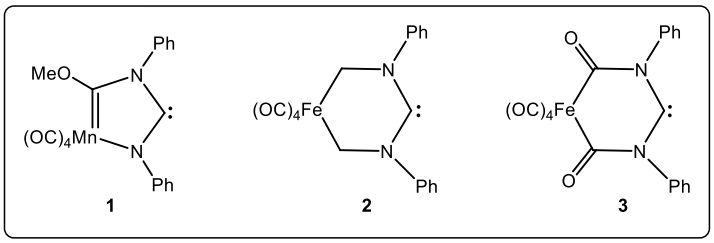

Scheme 2.2.1: Schematic representation of the MNHCs considered in this study.

[2.2.2] Computational Details

Density functional theory calculations were carried out to optimize all the molecules without any geometrical constraints by using meta-GGA M06 [68] exchange–correlation functional in conjunction with the valence polarized def2-TZVP basis set for all the elements [69,70]. Frequency calculations were carried out at the same level of theory to check the nature of the stationary points. All the molecules were found to be minima with real vibrational frequencies. In addition, TDDFT calculations were performed at the same level of theory to obtain the HOMO–LUMO gap in terms of the excitation energies. The transition states were characterized by the presence of only one imaginary

frequency which was further confirmed by performing the intrinsic reaction coordinate (IRC) analysis at the same level of theory. Dispersion effects were incorporated by using the D3 version of Grimme's dispersion correction coupled with the original D3 damping function with the keyword Empiricaldispersion = GD3 [71]. Further, solvent (Toluene) effects were incorporated by using the polarizable continuum model, PCM [72]. The ultrafine integration grid was used for all the calculations. Bonding analysis was performed with the help of NBO routine [73,74] as implemented in the Gaussian 09 suit of programs [75]. The energetics were evaluated considering change in Gibbs free energies at 298 K and 1 atm pressure unless otherwise specified.

[2.2.3] Results and Discussion

The singlet state optimized geometries of **1–3** possess a slightly distorted central ring with the ∠N–C_C–N angle (C_C = carbenic carbon) varying from 109.2°–120.7° (Figure 2.2.1). The central ring of **1** is slightly distorted while that of **3** is planar. The metallacyclic ring of **2** is distorted due to the presence of sp^3 hybridized carbon atom. Moreover, while **1** possesses two different C_C–N bond lengths, both **2** and **3** exhibits similar C_C–N bond lengths (Figure 2.2.1). The thermodynamic stability of the MNHCs was gauged by evaluating their singlet–triplet energy separation (ΔE_{S-T}) values (Figure 2.2.2) [76, 77]. For the sake of comparison, Figure 2.2.2 also includes the ΔE_{S-T} values of some experimentally known carbenes. It was found that all of the MNHCs explored here exhibit a stable singlet ground state. Furthermore, we have calculated (at the same level of theory) the ΔE_{S-T} values for the experimentally trapped MNHCs reported by Ruiz and coworkers [59] (Table 2.2.1) which were found to be significantly lower than those obtained for **1–3** (36.2–46.4 kcal mol^{-1}, Figure 2.2.2). This indicates **1–3** may be stable enough for experimental realization. The thermodynamic stabilities of **1–3** were further probed by evaluating their hydrogenation energies (E_{Hydro}, Figure 2.2.2). In general, the lower the exothermicity of the hydrogenation reaction, the higher will be the thermodynamic stability of the carbene under consideration. Indeed, the highest exothermicity (E_{hydro}) is obtained for MNHC **3** that has the lowest computed ΔE_{S-T} value (Figure 2.2.2). The same is true for the parent carbenes, i.e., **I** with the highest ΔE_{S-T} value possess the lowest hydrogenation energy. Furthermore, all the MNHCs exhibit a lower HOMO–LUMO energy gap (ΔE_{H-L}) (Figure 2.2.2) than their corresponding parent carbenes signifying their higher reactivity.

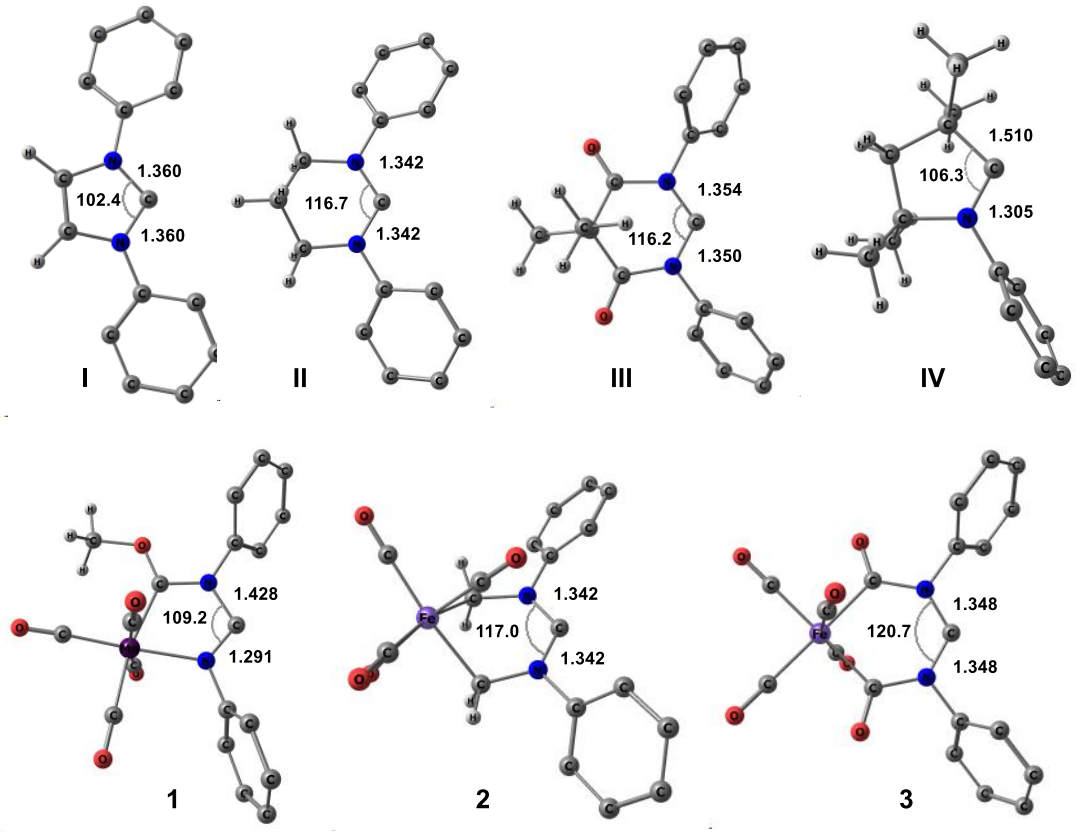

Figure 2.2.1: Singlet state optimized geometries of **I–IV** and **1–3** at M06-D3/def2-TZVP (Toluene) level of theory. The hydrogen atoms of the phenyl rings are omitted for clarity.

Table 2.2.1: Calculated (M06-D3/def2-TZVP (Toluene)) ΔE_{S-T} values (in kcal mol^{-1}) for the experimentally trapped MNHCs (bipy = bipyridine).

Sl. No.	Molecules	ΔE_{S-T}
1	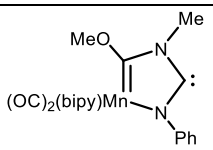	27.2
2	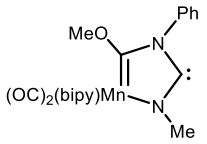	24.6
3	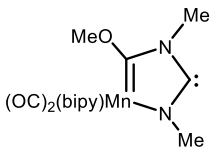	24.2

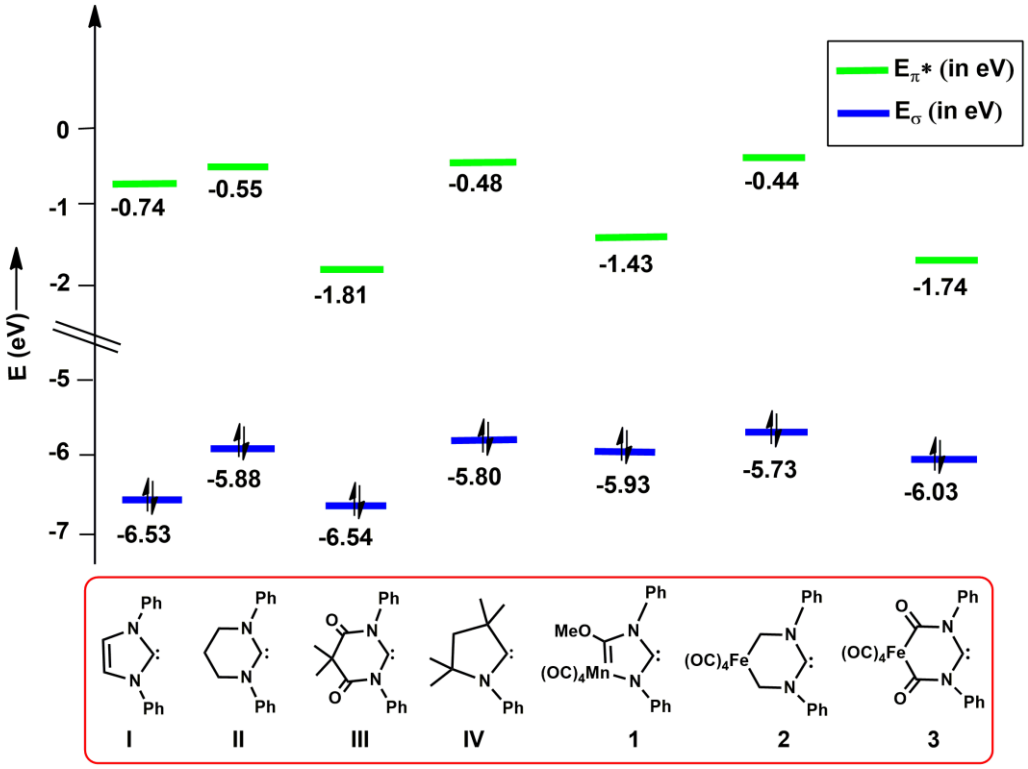

	I	II	III	IV	1	2	3
$\Delta E_{S\text{-}T}$ (kcal mol^{-1})	69.2	53.4	43.7	42.7	43.6	46.4	36.2
$\Delta E_{H\text{-}L}$ (eV)	5.78	5.33	4.73	5.32	4.51	4.68	4.29
	4.41	*3.86*	*3.13*	*3.68*	*3.03*	*3.61*	*2.78*
E_{Hydro} (kcal mol^{-1})	-23.3	-32.1	-46.9	-50.6	-32.0	-40.0	-50.8

Figure 2.2.2: Calculated (M06-D3/def2-TZVP (Toluene)) energies (in eV) of the σ-symmetric (donor) and π-symmetric (acceptor) molecular orbitals concentrated at the carbene carbon of MNHCs **1–3** and NHCs **I–IV**. Also given are the values of singlet-triplet ($\Delta E_{S\text{-}T}$), HOMO-LUMO gap ($\Delta E_{H\text{-}L}$) and hydrogenation energies (E_{Hydro}). The values given in italics correspond to HOMO-LUMO gaps in terms of the excitation energies obtained from TDDFT calculations at the same level of theory.

The electron donor and acceptor abilities of MNHCs **1–3** were judged by evaluating the energies of their occupied σ-and unoccupied π-symmetric molecular orbitals centered at the carbene carbon (Figure 2.2.2). It can be ascertained from Figure 2.2.2 that **1–3** exhibits superior electron donor ability compared to the NHCs **I–III** which is in accord with previous studies [58,59] and may be attributed to inductive destabilization of the carbenic lone pair as the valence shell of the neighboring amino nitrogen atoms gets saturated by withdrawal of electron density from the electron rich metal fragments. Also, the carbenic lone pairs of **1–3** possess less s character (46.1%,

40.9% and 41.5% in **1**, **2** and **3** respectively) than the parent carbenes **I–III** (49.0%, 41.4% and 44.5% in **I**, **II** and **III** respectively). Surprisingly, the π acceptance ability of **1** is substantially greater (almost twice) than that of **I** which may be attributed to the significant stabilization of the formally vacant p_π (π^*) orbital at C_C in **1**. The stabilization of the π^* orbital (lower E_π^* value) may be credited to reduced transfer of electron density from the lone pair orbital of one of the N atom (the N atom that is bonded to the backbone C atom). This is corroborated not only from the longer C_C–N bond in **1** (C_C–N bond lengths of 1.428 and 1.360 Å in **1** and **I** respectively) but also from significantly lower occupancy of the vacant p_π orbital at C_C in **1** (ca. occupancies of 0.574 and 0.688 in **1** and **I** respectively). In addition, while the HOMO corresponds to the σ-symmetric donor orbital for all the MNHCs **1–3**, it is only **1** and **3** where the π-symmetric acceptor orbital corresponds to the LUMO. On the other hand for **2**, the LUMO is not the π-symmetric acceptor orbital – rather, it is the higher lying LUMO+7 orbital indicating that this orbital is unlikely to play any role in determining the π-acidity [78]. Normally in carbenes that are capable of small molecule activation, the HOMO represents the σ-symmetric donor orbital while the LUMO represents the π-symmetric acceptor orbital [78]. Since in compound **2**, the LUMO do not represent such an orbital therefore **2** is not considered for further discussion. Furthermore, it is indeed encouraging to note that the ligand properties of **1** and **3** (Figure 2.2.2) are comparable to those of DAC (**III**) and CAAC (**IV**) which are known for their remarkable activity in small molecule activation [40,41,47,52,56].

[2.2.3.1] Activation of Dihydrogen

The mechanism of H_2 activation by ambiphilic carbenes is already well established [40, 79] in which the carbene lone pair interacts with the H_2 antibonding orbital. As a result of this interaction, a hydridic hydrogen ($H^{\delta-}$) is formed which eventually moves toward the carbenic vacant p_π orbital to yield the desired dihydrogen scission product. The overall reaction proceeds via a transition state (TS) featuring a significantly elongated and polarized H–H bond. Accordingly, we have searched for the probable TS involved in the activation of H_2 by our computationally designed MNHCs, **1** and **3**.

The reaction profile and the optimized geometries of the TSs (**1TS$^{H–H}$** and **3TS$^{H–H}$**) obtained for the activation of H_2 by **1** and **3** are shown in Figure 2.2.3. It is obvious

from Figure 2.2.3 that both the TSs exhibit a considerably elongated (1.091–1.249 Å) and polarized (Table 2.2.2) H–H bond, with the positively polarized hydrogen atom being already strongly bonded to the C_C (WBI = 0.615–0.651) while the hydridic hydrogen ($H^{\delta-}$) remains distant from the C_C. Nonetheless, the calculated C_C–$H^{\delta-}$ distances (2.009–2.217 Å) and their WBI values (0.312–0.413) indicate the presence of substantial bonding interaction between the C_C and the $H^{\delta-}$ which is eventually captured by the C_C to yield the desired H–H splitting product. In addition, an increase in the occupancies of the formally vacant p_π orbital centered at the C_C of **1TS$^{H–H}$** and **3TS$^{H–H}$** (Table 2.2.2) from their respective parent MNHCs (ca. occupancies of 0.574 and 0.486 for **1** and **3** respectively) further corroborate the presence of considerable bonding interaction between the C_C and hydridic hydrogen. A comparison of the geometrical parameters of the TSs (Table 2.2.2) **1TS$^{H–H}$** and **3TS$^{H–H}$** with their corresponding parent MNHCs (Figure 2.2.1) shows that there are no appreciable change in their computed C_C–N bond lengths however, they exhibit slightly larger ∠N-C_C-N angle.

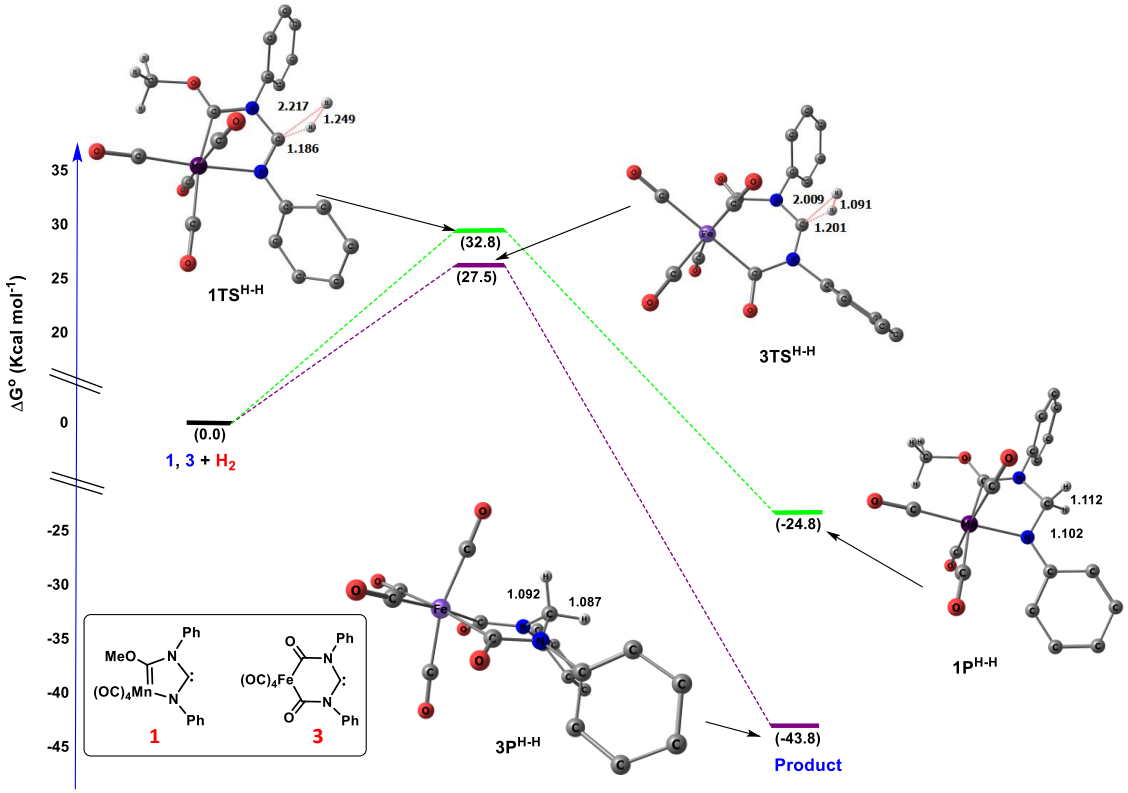

Figure 2.2.3: Energy profile diagram for the activation of hydrogen by **1** and **3** at M06-D3/def2-TZVP (Toluene) level of theory. The hydrogen atoms of the phenyl rings are omitted for clarity.

Table 2.2.2: Calculated(M06-D3/def2-TZVP (Toluene)) important geometrical parameters and natural charges at hydridic ($q_H^{\delta-}$) and positively polarized hydrogen atom ($q_H^{\delta+}$) and occupancies of the formally vacant p_π orbital at the carbene center (Occ_{P_π}) of the transition states involved in the activation of hydrogen by **1**, **3** and **IV** (CAAC). Bond lengths, bond angles (∠N-C_C-X, X = C, N) are given in Å and in degree (°) respectively and Wiberg Bond Index (WBI) values are given within parentheses.

Molecules	$H^{\delta+} - H^{\delta-}$	$C_C - H^{\delta-}$	$C_C - H^{\delta+}$	C_C-X	∠N-C_C-X	$q_H^{\delta-}$	$q_H^{\delta+}$	Occ_{P_π}
IVTS^{H-H}	1.076 (0.314)	1.950 (0.465)	1.214 (0.621)	1.325/1.502 (1.298)/(0.997)	108.0	-0.196	0.185	0.756
1TS^{H-H}	1.249 (0.266)	2.217 (0.312)	1.186 (0.651)	1.297/1.403 (1.497)/(1.004)	114.0	-0.423	0.206	0.815
3TS^{H-H}	1.091 (0.320)	2.009 (0.413)	1.201 (0.615)	1.353/1.353 (1.155)/(1.154)	124.1	-0.197	0.179	0.770

The calculated activation free energy barrier ($\Delta G°_{TS}^{H-H‡}$) for **1** and **3** are found to be 32.8 and 27.5 kcal mol^{-1} (Table 2.2.3) respectively. The superior reactivity of **3** compared to **1** may be attributed to its lower ΔE_{S-T} and ΔE_{H-L} values [40, 48, 80]. Furthermore, it should be noted that the barriers obtained for activation of H_2 by **1** and **3** are found to be comparable (28.7 kcal mol^{-1}) to that for CAAC (**IV**) implying that these computationally designed MNHCs are ideal candidates for H_2 activation under ambient conditions. Also, the calculated reaction free energies ($\Delta G°_{Total}^{H-H}$) are found to be substantially exergonic (Table 2.2.3) further, implying the feasibility of the reaction. Furthermore, it should be noted that the H–H splitting products obtained from **1** and **3** exhibits highly distorted central ring with elongated N-C bond lengths as well as a smaller ∠N–C–N bond angle (108.6°-114.4°) from their respective parent MNHCs (Figure 2.2.1). The optimized geometries of the TS and H–H splitting product obtained for **IV** is shown in Figure 2.2.4.

Table 2.2.3: Calculated (M06-D3/def2-TZVP (Toluene)) activation energy barrier ($\Delta G°_{TS}^{H-H‡}$, in kcal mol^{-1}) and reaction free energies ($\Delta G°_{Total}^{H-H}$, kcal mol^{-1}) for the activation of hydrogen.

Molecules	$\Delta G°_{TS}^{H-H‡}$	$\Delta G°_{Total}^{H-H}$
IV	28.7	-43.0
1	32.8	-24.8
3	27.5	-43.8

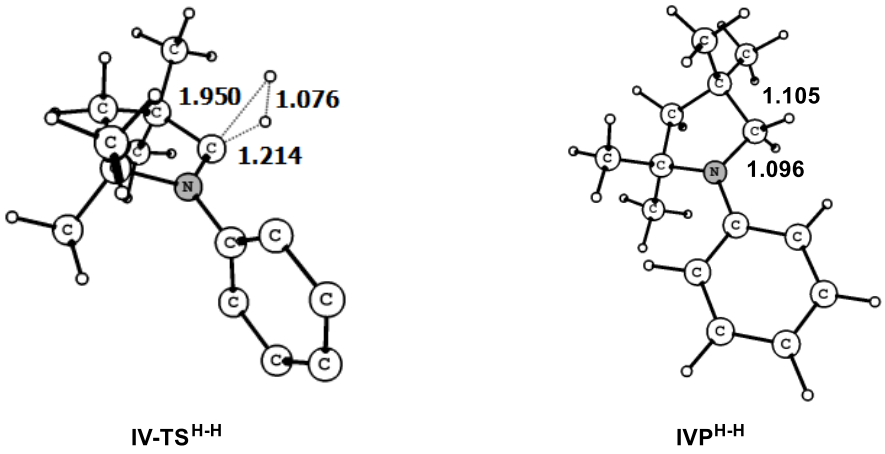

Figure 2.2.4: Optimized geometries of the TS and H–H splitting product obtained CAAC (**IV)** at M06-D3/def2-TZVP (Toluene) level of theory.

[2.2.3.2] Activation of Ammonia

Activation of NH_3 by TM compounds is a challenging task as they tend to favor the formation of classical Warner-type amine complexes [81]. However, carbenes are found to be capable of activating NH_3 under ambient conditions [40,55,82]. Generally, both nucleophilic or electrophilic reaction pathways can be envisaged for the activation of NH_3 by carbenes (Scheme 2.2.2) [83]. Typically, carbenes including CAACs follow the nucleophilic pathway in which the carbene lone pair (σ_{LP}) delocalizes to one of the

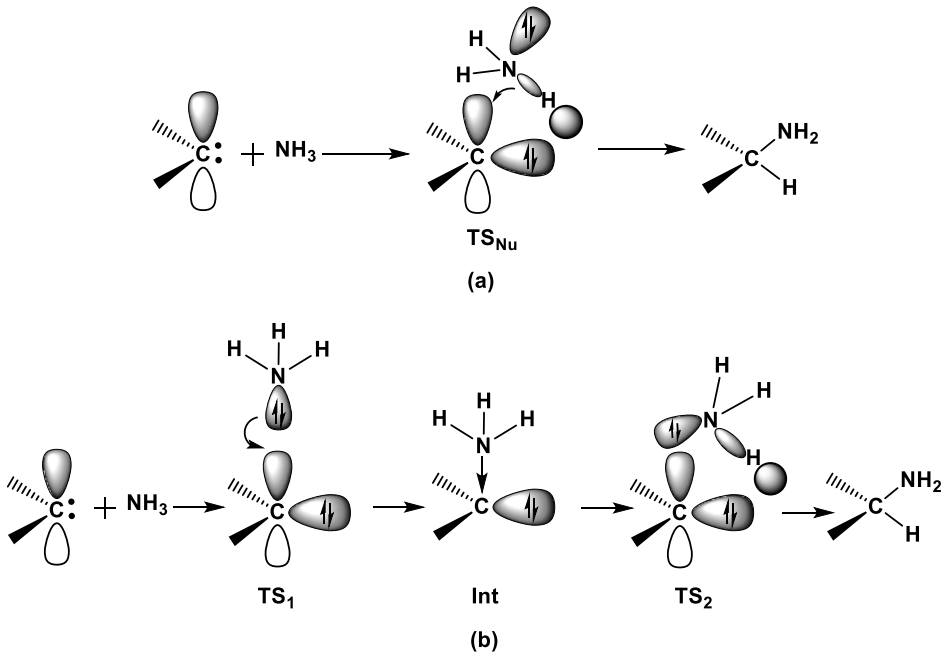

Scheme 2.2.2: Schematic representation for activation of NH_3 by carbene via (a) nucleophilic and (b) electrophilic pathway.

N–H antibonding orbital of NH_3 to induce sufficient polarization to the corresponding N–H bond [40,79]. As a result of this interaction, a pseudo amide ($NH_2^{\delta-}$) like fragment is formed which eventually moves toward the vacant p_π orbital at C_C to yield the desired N–H bond splitting product. The overall process proceeds via a TS featuring an appreciably elongated and polarized N–H bond.

The optimized geometries of the TSs as well as the reaction profile for the activation of NH_3 by **1** and **3** via nucleophilic pathway are represented in Figure 2.2.5. Both the TSs, $\mathbf{1TS_{Nu}^{N-H}}$ and $\mathbf{3TS_{Nu}^{N-H}}$ exhibit a significantly elongated (1.539–1.688 Å) and polarized (Table 2.2.4) N–H bond with the positively polarized hydrogen ($H^{\delta+}$) atoms already strongly bound to the C_C (WBI = 0.689–0.743) while the pseudo amide ($NH_2^{\delta-}$) like fragments remain distant from the C_C. However, the calculated C_C–$NH_2^{\delta-}$ distances (2.384–2.486 Å) and their corresponding WBI values (0.296–0.410) corroborate the presence of substantial bonding interaction between the C_C and the $NH_2^{\delta-}$ groups. This interaction is further corroborated from the increase in the occupancies of the formally vacant p_π orbital centered at the C_C of $\mathbf{1TS_{Nu}^{N-H}}$ and

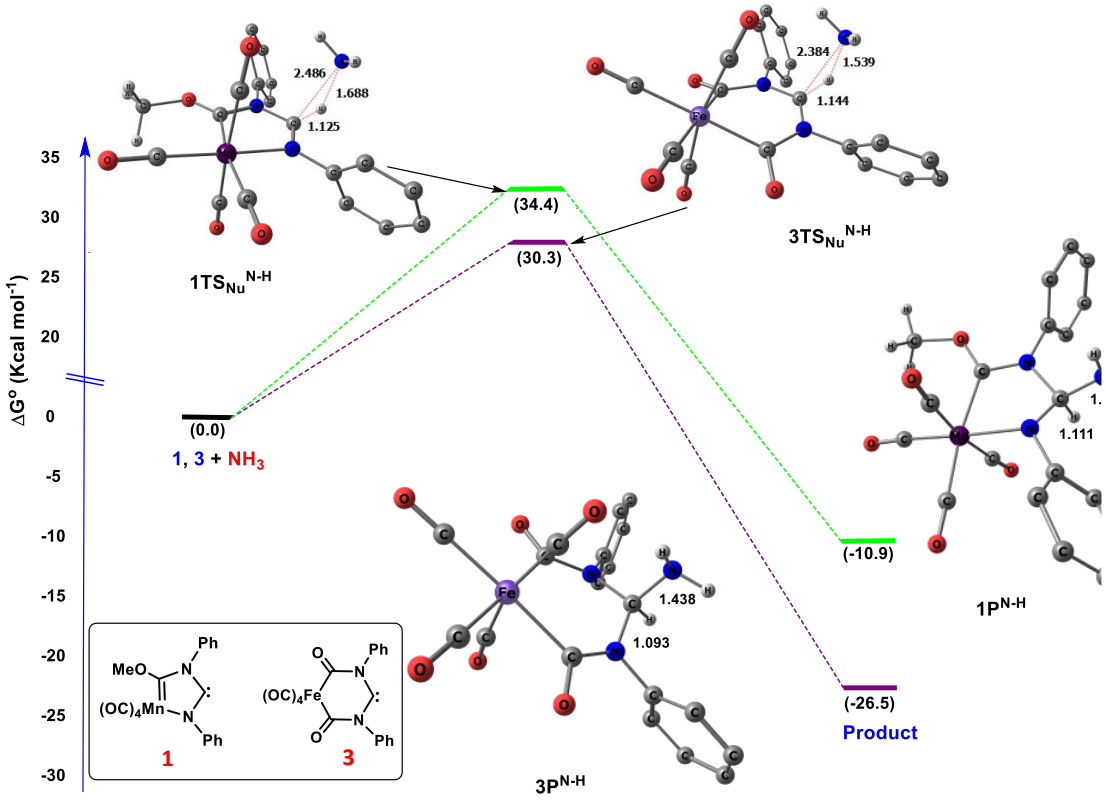

Figure 2.2.5: Energy profile diagram for the activation of N–H bond of NH_3 by **1** and **3** via nucleophilic pathway at M06-D3/def2-TZVP (Toluene) level of theory. The hydrogen atoms of the phenyl rings are omitted for clarity.

$3TS_{Nu}^{N–H}$ (Table 2.2.4). A comparison of the computed geometrical parameters of the TSs, **$1TS_{Nu}^{N–H}$** and **$3TS_{Nu}^{N–H}$** with their respective parent MNHCs shows that all the TS computes slightly larger ∠N–C_C–N angle with no appreciable changes in their calculated C_C–N bond lengths (Table 2.2.4) from their corresponding parent MNHCs (Figure 2.2.1). Further, it should be noted that in both the TSs, **$1TS_{Nu}^{N–H}$** and **$3TS_{Nu}^{N–H}$** the lone pair at the nitrogen atom points away from the carbenic p_π orbital (Figure 2.2.6) thereby supporting the nucleophilic mode of activation [40].

The calculated activation energy barrier ($\Delta G°_{TS_{Nu}}{}^{N\text{-}H^{\ddagger}}$) values for **1** and **3** are found to be 34.4 and 30.3 kcal mol^{-1} (Table 2.2.5) respectively and they are found to be close to those obtained for experimentally evaluated DAC (**III**, 31.3 kcal mol^{-1}) and CAAC (**IV**, 30.5 kcal mol^{-1}) indicating that **1** and **3** are also potential for activation of N–H bonds. Similar to the H_2 activation, **3** once again exhibits superior reactivity compared to **1** which may be attributed to its lower $\Delta E_{S\text{-}T}$ and $\Delta E_{H\text{-}L}$ values. Also, the calculated reaction free energy ($\Delta G°_{Total}{}^{N\text{-}H}$) values are found to be appreciably exergonic (Table 2.2.5) implying the feasibility of the reaction. However, the moderately higher barrier height obtained for **1** suggests the requirement of slightly elevated reaction conditions to achieve the N–H bond cleaved product.

Table 2.2.4: Calculated (M06-D3/def2-TZVP (Toluene)) important geometrical parameters and natural charges at the nitrogen atom of the $NH_2^{\delta-}$ fragment ($q_{NH_2}{}^{\delta-}$) and hydrogen atom ($q_H{}^{\delta+}$) and occupancies of the formally vacant p_π orbital at the carbene center (Occ_{P_π}) of the transition states involved in the activation of N–H bond of NH_3 by **1**, **3**, DAC (**III**) and CAAC (**IV**) via nucleophilic pathway. Bond lengths, bond angles (∠N-C_C-X, X = C, N) are given in Å and in degree (°) respectively and Wiberg Bond Index (WBI) values are given within parentheses.

Molecule	**$H_2N^{\delta-}$–$H^{\delta+}$**	**C_C–$NH_2^{\delta-}$**	**C_C–$H^{\delta+}$**	**C_C-X**	**∠N-C_C-X**	**$q_{NH_2}{}^{\delta-}$**	**$q_H{}^{\delta+}$**	**Occ_{P_π}**
$IIITS_{Nu}^{N\text{-}H}$	1.513 (0.185)	2.332 (0.436)	1.149 (0.681)	1.354/1.354 (1.160)/(1.160)	119.9	-1.080	0.333	0.745
$IVTS_{Nu}^{N\text{-}H}$	1.542 (0.177)	2.428 (0.401)	1.156 (0.695)	1.314/1.496 (1.378)/(0.995)	109.5	-1.165	0.324	0.792
$1TS_{Nu}^{N\text{-}H}$	1.688 (0.117)	2.486 (0.296)	1.125 (0.743)	1.294/1.397 (1.494)/(1.013)	115.0	-1.210	0.320	0.810
$3TS_{Nu}^{N\text{-}H}$	1.539 (0.176)	2.384 (0.410)	1.144 (0.689)	1.351/1.351 (1.176)/(1.176)	124.9	-1.110	0.329	0.749

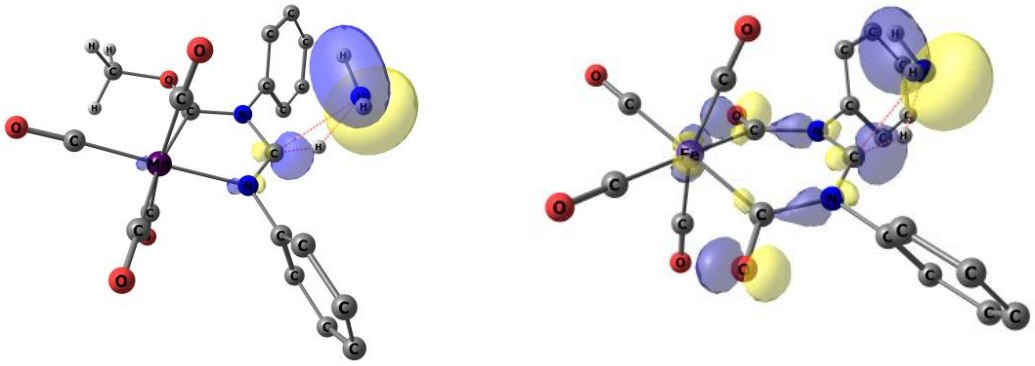

$1TS_{Nu}^{N-H}$ $3TS_{Nu}^{N-H}$

Figure 2.2.6: Molecular orbitals showing the orientation of the nitrogen lone pair for the TSs, $\mathbf{1TS_{Nu}^{N-H}}$ and $\mathbf{3TS_{Nu}^{N-H}}$ involved in the activation of N–H bond of NH_3 via nucleophilic pathway. The hydrogen atoms of the phenyl rings are omitted for clarity.

Table 2.2.5: Calculated (M06-D3/def2-TZVP (Toluene)) activation energy barrier (kcal mol^{-1}) for the nucleophilic ($\Delta G°_{TS_{Nu}}^{N-H‡}$) and electrophilic ($\Delta G°_{TS_1}^{N-H‡}$and $\Delta G°_{TS_2}^{N-H‡}$) pathways, reaction free energies (kcal mol^{-1}) for the formation of the intermediate ($\Delta G°_{Int}^{N-H}$) and N–H splitting product ($\Delta G°_{Total}^{N-H}$). The values given within parenthesis corresponds to those with respect to the starting reactants for the second transition state (TS_2^{N-H}) involved in the electrophilic pathway.

Molecules	$\Delta G°_{TS_{Nu}}^{N-H‡}$	$\Delta G°_{TS_1}^{N-H‡}$	$\Delta G°_{Int}^{N-H}$	$\Delta G°_{TS_2}^{N-H‡}$	$\Delta G°_{Total}^{N-H}$
III	31.3	18.9	19.8	12.5 (32.3)	-26.9
IV	30.5	-	-	-	-26.4
1	34.4	-	-	-	-10.9
3	30.3	20.8	21.0	10.1 (31.1)	-26.5

On the other hand, NH_3 activation via an electrophilic pathway involves two steps (Scheme 2.2.2) [83]. The first step involves adduct formation via interaction between the amine lone pair (LP_N) and the vacant p_π orbital at C_c. However, we have determined that only the most π-acidic MNHC **3** can form a metastable adduct with NH_3, thus ruling out the possibility of an electrophilic activation of NH_3 by **1**. For the sake of comparison we have also included the experimentally evaluated strongly electrophilic DAC (**III**) in our discussion. The adduct formation of **3** with NH_3 ($\mathbf{3Int^{N–H}}$, Figure 2.2.7) proceeds via a TS ($\mathbf{3TS_1^{N–H}}$) with an activation barrier ($\Delta G°_{TS_1}^{N-H‡}$) of 20.8 kcal mol^{-1} (**III**, $\Delta G°_{TS_1}^{N-H‡}$= 18.9 kcal mol^{-1}, Table 2.2.5). The different electronic and geometric

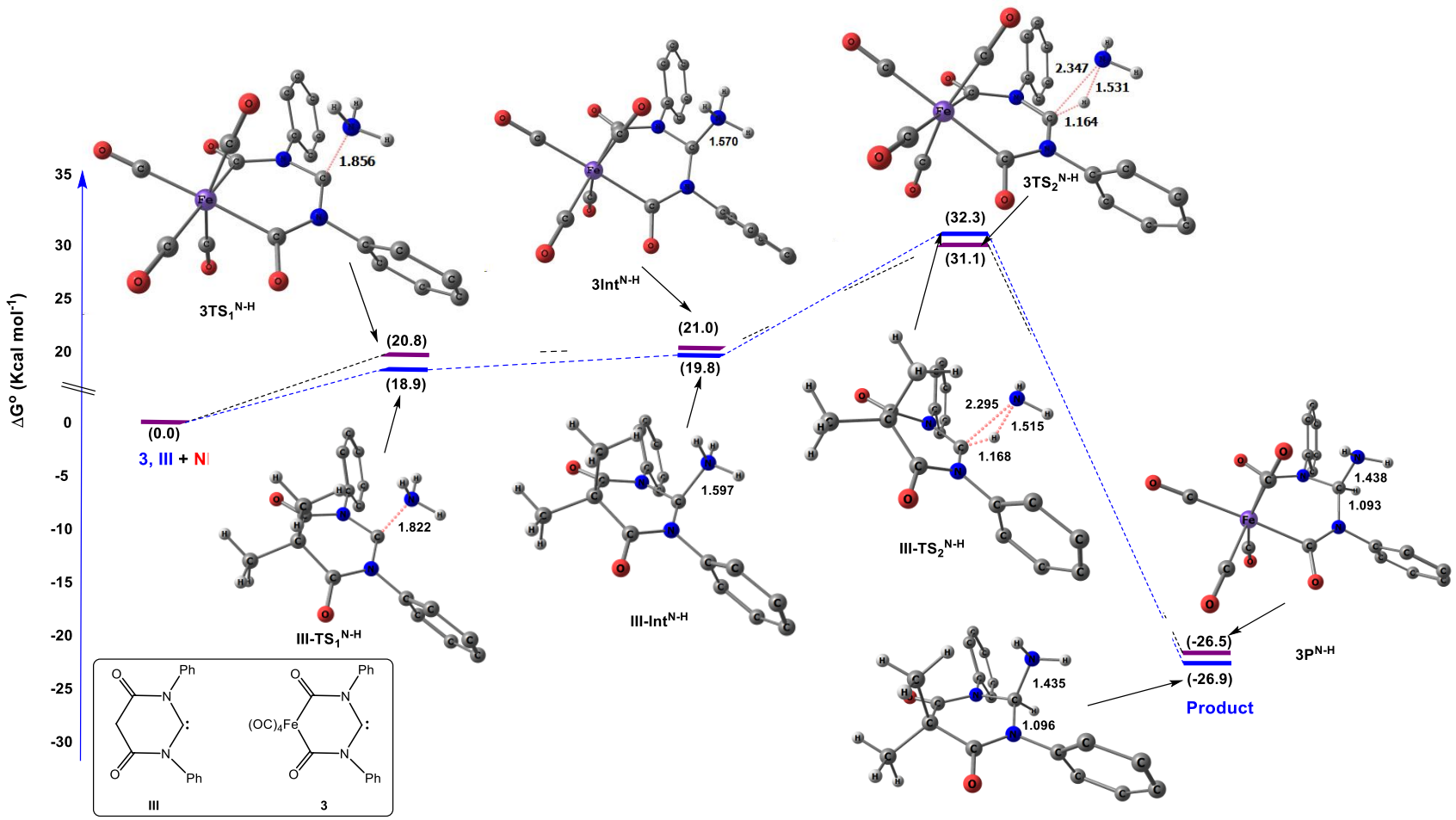

Figure 2.2.7: Energy profile diagram for the activation of N–H bond of NH_3 by **3** via electrophilic pathway at M06-D3/def2-TZVP (Toluene) level of theory. The hydrogen atoms of the phenyl rings are omitted for clarity.

parameters associated with **3TS$_1^{N–H}$** and **3Int$^{N–H}$** are given in Table 2.2.6. The formation of the intermediate is found to be endergonic by 21.0 kcal mol^{-1} (**III**, $\Delta G°_{Int}{}^{N-H}$ = 19.8 kcal mol^{-1}). There is incipient activation of one of the N–H bond in **3TS$_1^{N–H}$** (N–H bond length of 1.020 Å compared to 1.014 Å for the other two N–H bonds) which also features a C_C–N bond of 1.856 Å having a WBI of 0.515 (Table 2.2.6) indicating substantial interaction between LP_N and p_π orbital at C_C. This interaction is further evident from the increase and decrease in the occupancies of the formally vacant p_π orbital centered at C_C of **3TS$_1^{N–H}$** (0.574) and LP_N (1.633) respectively, from the parent MNHC **3** (0.486) and free NH_3 (1.997) (Table 2.2.6). Interaction of σ_{LP} with the $\sigma^*_{N–H}$ orbital further stretches the N–H bond to 1.031 Å in **3Int$^{N–H}$** which can also be corroborated from the NBO based second order perturbation analysis yielding stabilization energies of 4.6 and 8.5 kcal mol^{-1} in **3TS$_1^{N–H}$** and **3Int$^{N–H}$** respectively. In the second step, **3Int$^{N–H}$** undergoes an intramolecular rearrangement via **3TS$_2^{N–H}$** with an activation energy barrier of 10.1 kcal mol^{-1} (**III**,

Table 2.2.6: Calculated (M06-D3/def2-TZVP (Toluene)) important geometrical parameters and natural charges at the nitrogen atom of NH_3 (q_{NH_3}) and carbenic carbon (q_{Cc}) and occupancies of the formally vacant p_π orbital at the carbene center (Occ_{P_π}) of the first transition state (**TS$_1^{N-H}$**) and the intermediate (**Int^{N-H}**) involved in the activation of N**–**H bond of NH_3 by **3** and DAC (**III**) via electrophilic pathway. Bond lengths, bond angles (∠N-C_c-N) are given in Å and in degree (°) respectively and Wiberg Bond Index (WBI) values are given within parentheses.

Molecules	**$H_3N – C_c$**	**C_c-N**	**∠N-C_c-N**	**q_{NH_3}**	**q_{Cc}**	**Occ_{P_π}**
III-TS$_1^{N-H}$	1.822 (0.547)	1.407/ 1.407 (1.020)/(1.020)	113.3	-0.826	0.185	0.588
III-Int^{N-H}	1.597 (0.756)	1.425/1.425 (0.978)/(0.978)	113.3	-0.737	0.097	0.677
3TS$_1^{N-H}$	1.856 (0.515)	1.398/ 1.398 (1.041)/(1.042)	118.9	-0.843	0.199	0.574
3Int^{N-H}	1.570 (0.783)	1.417/ 1.417 (0.986)/(0.986)	119.1	-0.726	0.089	0.696

$\Delta G°_{TS_2}{}^{N\text{-}H^{\ddagger}}$ = 12.5 kcal mol^{-1}) to yield the desired N–H scission product. The N–H bond splitting is facilitated by effective interaction of the σ_{LP} with the σ^*_{N-H} orbital thereby generating a pseudo amide like fragment which is captured by the C_C. **3TS$_2^{N-H}$** features a significantly elongated and polarized N–H bond (Table 2.2.7) with the positively polarized hydrogen atom being bonded to C_c (WBI = 0.657) and the amide fragment interacting with C_c (WBI = 0.348). Further, it should be noted that in **3TS$_2^{N-H}$** the lone pair orbital at the nitrogen atom orient towards the carbenic vacant p_π orbital (Figure 2.2.8) thereby supporting the electrophilic mode of activation. Furthermore, we did not observe any appreciable changes in the calculated C_C–N bond lengths of **3TS$_2^{N-H}$** compared to that in **3** but it exhibits appreciably larger ∠N–C_C–N bond angle (Table 2.2.7 and Figure 2.2.1).

Table 2.2.7: Calculated (M06-D3/def2-TZVP (Toluene)) important geometrical parameters and natural charges at the nitrogen atom of the $NH_2^{\delta-}$ fragment ($q_{NH_2}{}^{\delta-}$) and hydrogen atom ($q_H{}^{\delta+}$) and occupancies of the formally vacant p_π orbital at the carbene center (Occ_{P_π}) of the second transition state (**TS$_2^{N-H}$**) involved in the activation of N**–**H bond of NH_3 by **3** and DAC (**III**) via electrophilic pathway. Bond lengths, bond angles (∠N-C_c-N) are given in Å and in degree (°) respectively and Wiberg Bond Index (WBI) values are given within parentheses.

Molecules	**$H_2N^{\delta-}$–$H^{\delta+}$**	**C_C–$NH_2^{\delta-}$**	**C_C–$H^{\delta+}$**	**C_C-N**	**∠N-C_C-N**	**$q_{NH_2}{}^{\delta-}$**	**$q_H{}^{\delta+}$**	**Occ_{P_π}**
III-TS$_2^{N-H}$	1.515	2.295	1.168	1.350/1.350	119.8	-1.119	0.316	0.710
	(0.224)	(0.377)	(0.652)	(1.171)/(1.171)				
3TS$_2^{N-H}$	1.531	2.347	1.164	1.346/1.346	124.7	-1.144	0.313	0.709
	(0.218)	(0.348)	(0.657)	(1.192)/(1.192)				

It is worthwhile to mention that **3TS$_1^{N-H}$** lies at a slightly lower energy than **3Int^{N-H}** (Figure 2.2.7) which may be attributed to the marginal loss of entropy associated with the formation of **3Int^{N-H}** (-0.039 kcal mol^{-1}K^{-1}) compared to that of the **3TS$_1^{N-H}$** (-0.038 kcal mol^{-1}K^{-1}) [83]. Thus, it may be sensible to evaluate the activation barrier for the overall process with respect to the second TS (**3TS$_2^{N-H}$**) instead of the first one (**3TS$_1^{N-H}$**). Accordingly, the calculated energy barrier for the activation of NH_3 by **3** is found to be 31.1 kcal mol^{-1} (**III**, 32.4 kcal mol^{-1}). From the above discussion, it may be concluded that **1** can activate NH_3 only via the nucleophilic pathway. Interestingly, the energy barrier obtained

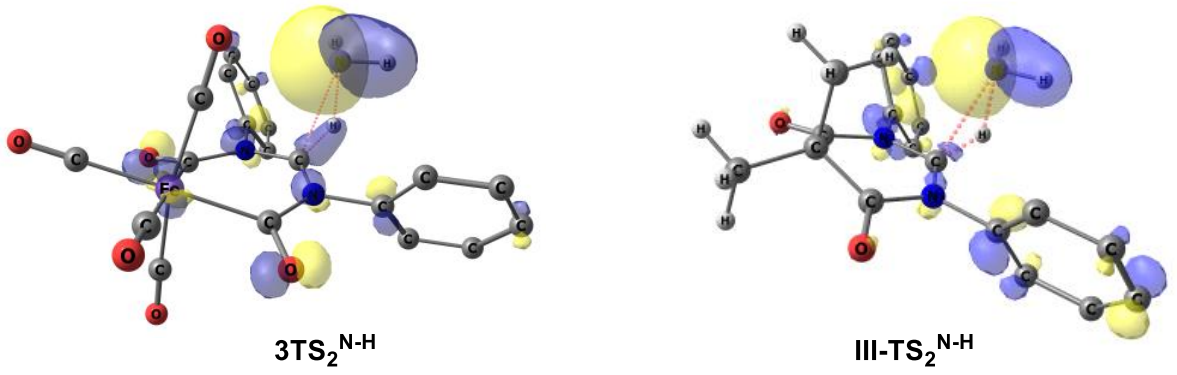

Figure 2.2.8: Molecular orbitals showing the orientation of the nitrogen lone pair for the TSs, **3TS$_2^{N-H}$** and **III-TS$_2^{N-H}$** involved in the activation of N–H bond of NH_3 via electrophilic pathway. The hydrogen atoms of the phenyl rings are omitted for clarity.

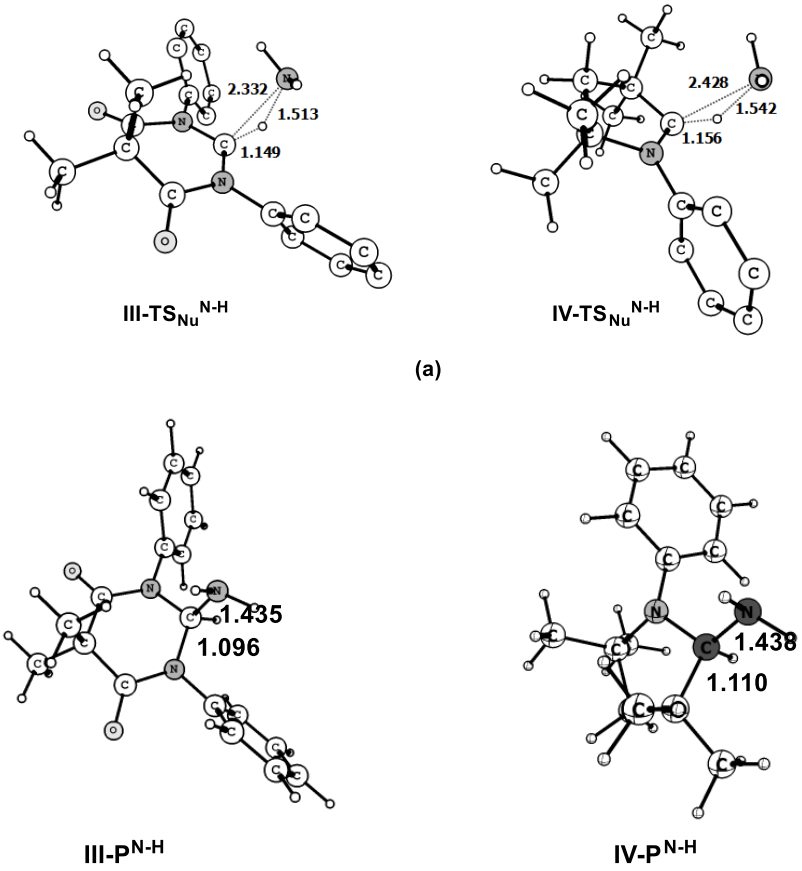

Figure 2.2.9: Optimized geometries ((M06-D3/def2-TZVP (Toluene))) of (a) TS and (b) N–H bond splitting product obtained for **III** and **IV** via nucleophilic pathway.

for **3** is found to be comparable for both the pathways indicating that both pathways could operate simultaneously. The optimized geometries of the TSs and N–H splitting products obtained for **III** and **IV** via nucleophilic pathway is shown in Figure 2.2.9.

[2.2.3.3] Activation of Phosphine

Similar to the NH_3 activation, here also both electrophilic and nucleophilic pathways are considered for the activation of PH_3 by **1** and **3**. The optimized geometries of the TSs (**1TS$_{Nu}^{P–H}$** and **3TS$_{Nu}^{P–H}$**) and the reaction profiles obtained for the nucleophilic mode of activation of PH_3 by **1** and **3** are shown in Figure 2.2.10. Furthermore, both the TSs (Figure 2.2.10) exhibit a significantly elongated and polarized P–H bond (Table 2.2.8). There is significant interaction between the proton and C_C as evident from the calculated WBI values (0.456–0.489, Table 2.2.8). There is also non-negligible interaction between the $PH_2^{\delta-}$ fragment and C_C (WBI values: 0.282–0.326, Table 2.2.8) which is evident from an increase in the occupancies of the formally vacant p_π orbital centered at C_C of **1TS$_{Nu}^{P–H}$** and **3TS$_{Nu}^{P–H}$** (Table 2.2.8). In addition, there is no appreciable change in the geometries of the metallacyclic rings of **1TS$_{Nu}^{P–H}$** and **3TS$_{Nu}^{P–H}$** compared to those in **1** and **3** (Table 2.2.8 and Figure 2.2.1). The proton and $PH_2^{\delta-}$ group gradually migrates toward the carbene center to yield the P–H bond splitting product. It is interesting to note that in both the TSs, the lone pair at the phosphorus atom points away from the vacant carbene p_π orbital (Figure 2.2.11) thereby supporting the nucleophilic mode of activation. The calculated activation energy barrier ($\Delta G°_{TS_{Nu}}^{P\text{-}H‡}$) for **1** and **3** are found to be 16.8 and 13.8 kcal mol^{-1} respectively (Table 2.2.9). The superior reactivity of **3** compared to **1** may once again be attributed to relatively lower singlet-triplet and HOMO-LUMO gaps (Figure 2.2.2). Interestingly, the calculated $\Delta G°_{TS_{Nu}}^{P\text{-}H‡}$ values are found to be very close to those obtained for DAC (**III**, 14.4 kcal mol^{-1}) and CAAC (**IV**, 15.7 kcal mol^{-1}) which are known to be capable of activating P–H bonds [43, 57]. Also, the calculated reaction free energy ($\Delta G°_{Total}^{P\text{-}H}$) values are highly exergonic in nature (Table 2.2.9) indicating that these proposed MNHCs could be suitable candidates for PH_3 activation.

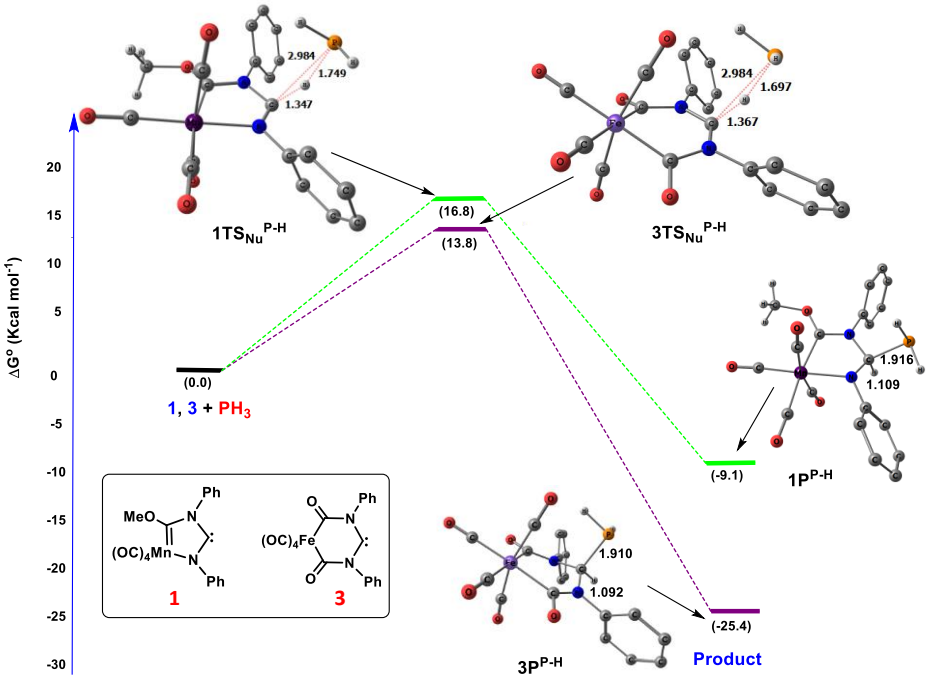

Figure 2.2.10: Energy profile diagram for the activation of P–H bond of PH_3 by **1** and **3** via nucleophilic pathway at M06-D3/def2-TZVP (Toluene) level of theory. The hydrogen atoms of the phenyl rings are omitted for clarity.

Table 2.2.8: Calculated (M06-D3/def2-TZVP (Toluene)) important geometrical parameters and natural charges at the phosphorus atom of the $PH_2^{\delta-}$ fragment ($q_{PH_2}^{\delta-}$) and hydrogen atom ($q_H^{\delta+}$) and occupancies of the formally vacant p_π orbital at the carbene center (Occ_{P_π}) of the transition states involved in the activation of P**–**H bond of PH_3 by **1**, **3**, DAC (**III**) and CAAC (**IV**) via nucleophilic pathway. Bond lengths, bond angles (∠N-C_C-X, X = C, N) are given in Å and in degree (°) respectively and Wiberg Bond Index (WBI) values are given within parentheses.

Molecules	**$H_2P^{\delta-}$–$H^{\delta+}$**	**C_C–$PH_2^{\delta-}$**	**C_C–$H^{\delta+}$**	**C_C-X**	**∠N-C_C-X**	**$q_{PH_2}^{\delta-}$**	**$q_H^{\delta+}$**	**Occ_{P_π}**
IIITS$_{Nu}^{P-H}$	1.708	2.931	1.338	1.354/1.356	118.4	-0.089	0.119	0.734
	(0.470)	(0.358)	(0.487)	(1.169)/(1.169)				
IVTS$_{Nu}^{P-H}$	1.733	3.030	1.376	1.310/1.507	108.5	-0.234	0.132	0.828
	(0.480)	(0.331)	(0.480)	(1.428)/(0.992)				
1TS$_{Nu}^{P-H}$	1.749	2.984	1.347	1.295/1.410	112.5	-0.232	0.135	0.801
	(0.461)	(0.282)	(0.489)	(1.519)/(0.992)				
3TS$_{Nu}^{P-H}$	1.697	2.984	1.367	1.349/1.348	123.4	-0.132	0.115	0.707
	(0.501)	(0.326)	(0.456)	(1.195)/(1.196)				

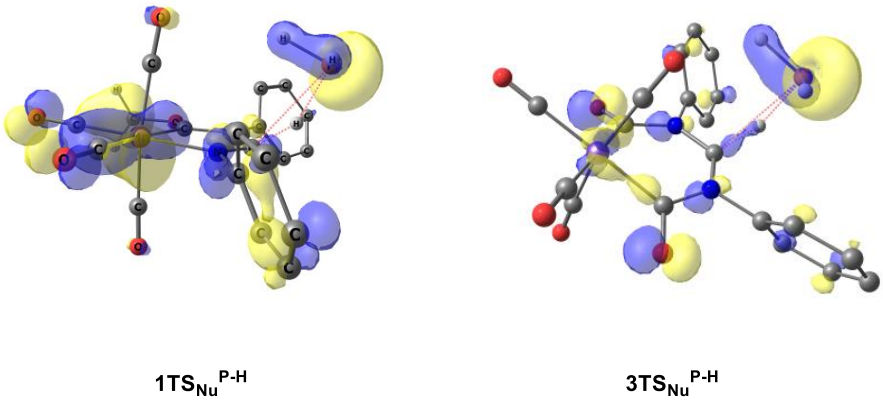

$1TS_{Nu}^{P-H}$ $3TS_{Nu}^{P-H}$

Figure 2.2.11: Molecular orbitals showing the orientation of the phosphorus lone pair for the TSs (**$1TS_{Nu}^{P-H}$** and **$3TS_{Nu}^{P-H}$**) involved in the activation of P**–**H bond of PH_3 via nucleophilic pathway. The hydrogen atoms of the phenyl rings are omitted for clarity.

As with the case of NH_3, electrophilic activation of PH_3 by **1** is not possible due to its lower electrophilicity. Activation of P–H bond is here considered for **3** along with DAC (**III**) so as to compare their relative efficiencies. As the mechanism of PH_3 activation is similar to that discussed for electrophilic NH_3 activation, here we will discuss only the major findings. In the first step, PH_3 forms an adduct with **3** (**$3Int^{P–H}$**) via a TS (**$3TS_1^{P–H}$**, Figure 2.2.12) with an activation energy barrier ($\Delta G°_{TS_1}{}^{P-H‡}$) of 12.3 kcal mol^{-1} (**III**, $\Delta G°_{TS_1}{}^{P-H‡}$= 11.7 kcal mol^{-1}, Table 2.2.9). The Gibbs energy for the formation of the intermediate ($\Delta G°_{Int}{}^{P-H}$) is calculated to be 8.4 kcal mol^{-1} (**III**, $\Delta G°_{Int}{}^{P-H}$ = 11.1 kcal mol^{-1}).

Table 2.2.9: Calculated (M06-D3/def2-TZVP (Toluene)) activation energy barrier (kcal mol^{-1}) for the nucleophilic ($\Delta G°_{TS_{Nu}}{}^{P-H‡}$) and electrophilic ($\Delta G°_{TS_1}{}^{P-H‡}$and $\Delta G°_{TS_2}{}^{P-H‡}$) pathways, reaction free energies (kcal mol^{-1}) for the formation of the intermediate ($\Delta G°_{Int}{}^{P-H}$) and P–H splitting product ($\Delta G°_{Total}{}^{P-H}$). The values given within parenthesis correspond to those with respect to the starting reactants for the second transition state ($TS_2{}^{N-H}$) involved in the electrophilic pathway.

Molecules	$\Delta G°_{TS_{Nu}}{}^{P-H‡}$	$\Delta G°_{TS_1}{}^{P-H‡}$	$\Delta G°_{Int}{}^{P-H}$	$\Delta G°_{TS_2}{}^{P-H‡}$	$\Delta G°_{Total}{}^{P-H}$
III	14.4	11.7	11.1	3.6 (14.7)	-26.1
IV	15.7	-	-	-	-29.3
1	16.8	-	-	-	-9.1
3	13.8	12.3	8.4	5.0 (13.4)	-25.4

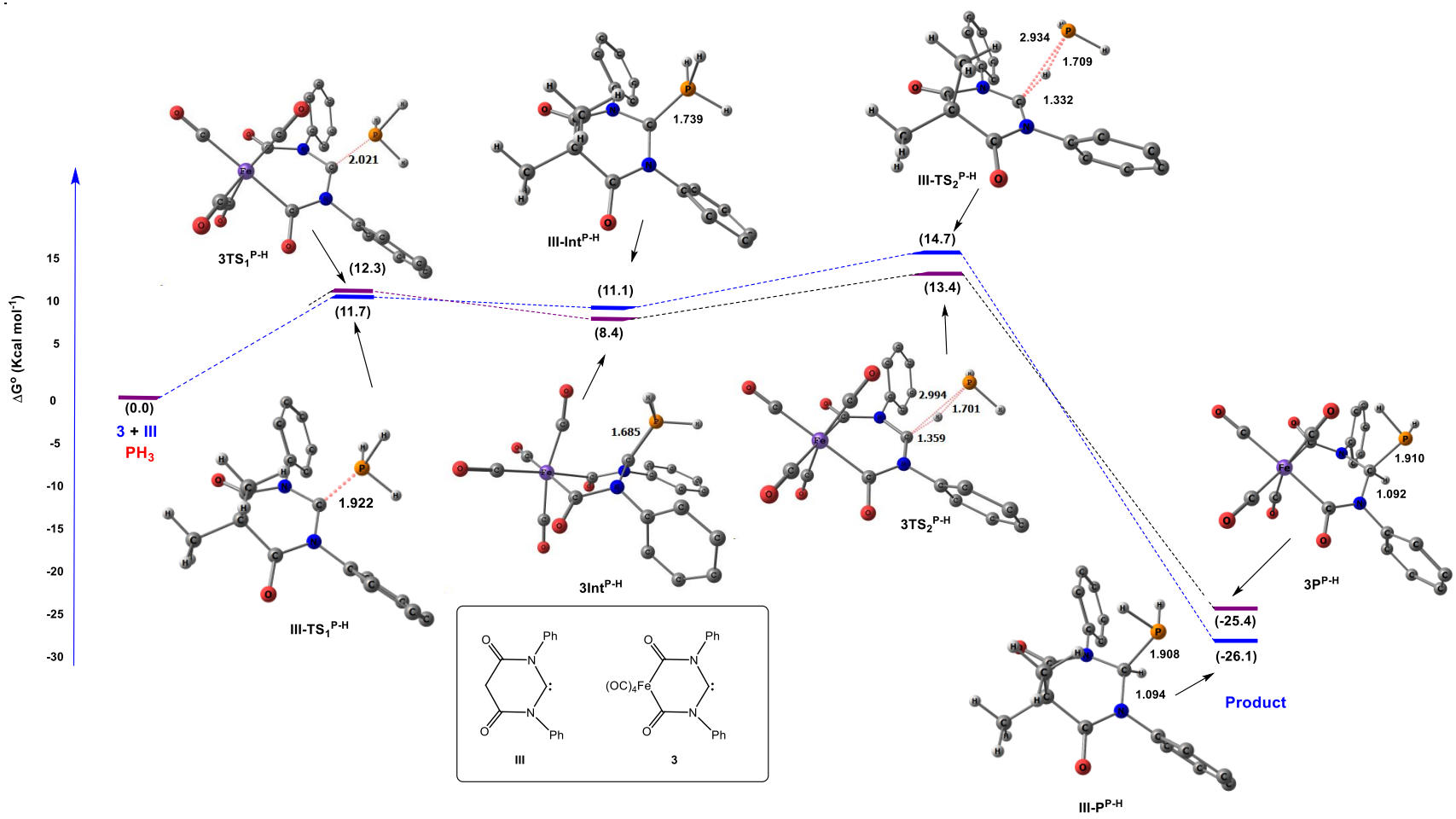

Figure 2.2.12: Energy profile diagram for the activation of P–H bond of PH_3 by **3** via electrophilic pathway at M06-D3/def2-TZVP (Toluene) level of theory. The hydrogen atoms of the phenyl rings are omitted for clarity.

In **3Int$^{P–H}$**, one of the P–H bond is found to be slightly elongated compared to the other two P–H bonds (1.423 Å vs. 1.402 Å) which may be attributed to interaction between σ_{LP} and $\sigma^*_{P–H}$ orbital. In the next step, **3Int^{P-H}** undergoes an intramolecular rearrangement via **3TS$_2^{P-H}$** having an activation energy barrier ($\Delta G°_{TS_2}{}^{P-H‡}$) of 5.0 kcal mol^{-1} (**III**, $\Delta G°_{TS_2}{}^{P-H‡}$ = 3.6 kcal mol^{-1}) to yield the final organophosphorus product. It may be noted that **3TS$_2^{P-H}$** features a 3c-2e interaction involving the σ_{LP}, proton and the $PH_2^{\delta-}$ fragment having considerable interaction between C_C and the $PH_2^{\delta-}$ fragment (WBI = 0.307). Also, in **3TS$_2^{P-H}$**, the P–H bond involved in the interaction with C_C is considerably stretched. Further, it should be noted that in **3TS$_2^{P-H}$** the lone pair orbital at the phosphorus atom is oriented towards the carbenic vacant p_π orbital (Figure 2.2.13) thereby supporting the electrophilic mode of activation. Thereafter, the eventual migration of the proton and the $PH_2^{\delta-}$ fragment from the activated P–H bond towards the C_C produced the desired P–H scission product. It is worth mentioning that energetically, **3TS$_2^{P-H}$** is similar to **3TS$_{Nu}^{P-H}$**, i.e., both lie at similar energies with respect to the starting reactants (**3** + PH_3). The optimized geometries of the TSs (via nucleophilic pathway) and P–H splitting products obtained for **III** and **IV** are shown in Figure 2.2.14.

Therefore, from the above discussion, it may be inferred that **1** can activate PH_3 only via nucleophilic pathway whereas the energy barrier obtained for **3** is found to be comparable for both the pathways implying that depending on the reaction conditions, one pathway may be favored over the other.

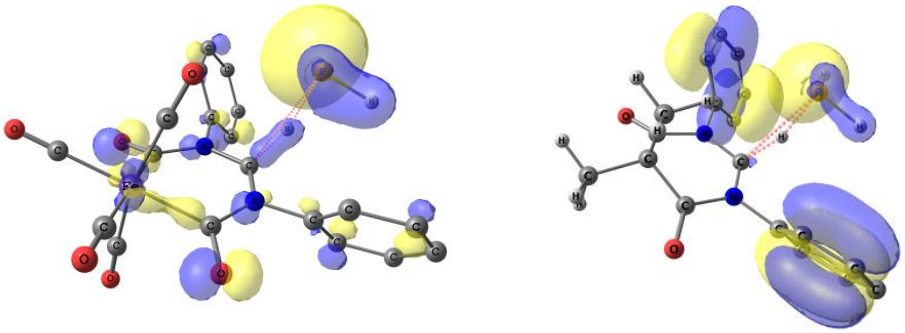

3TS$_2^{P-H}$ **III-TS$_2^{P-H}$**

Figure 2.2.13: Molecular orbitals showing the orientation of the phosphorus lone pair for the TSs, **3TS$_2^{P-H}$** involved in the activation of P–H bond of PH_3 via electrophilic pathway. The hydrogen atoms of the phenyl rings are omitted for clarity.

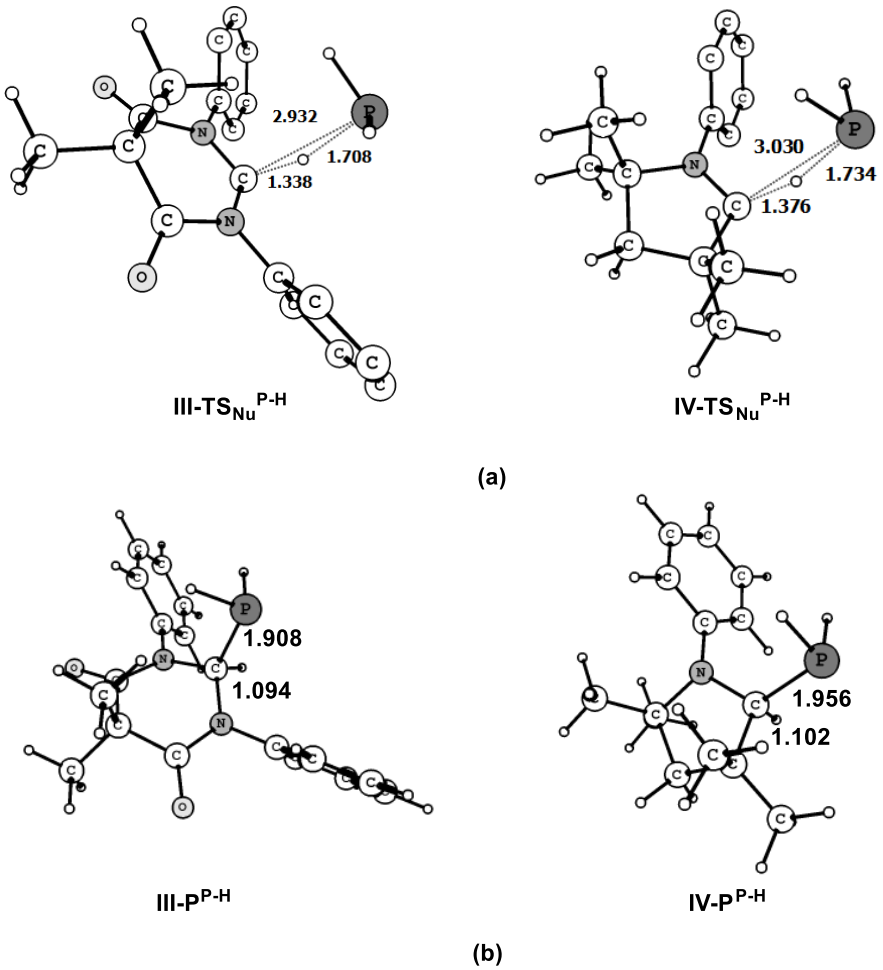

Figure 2.2.14: Optimized geometries (M06-D3/def2-TZVP (Toluene)) of the (a) TS and (b) P–H bond splitting product obtained for **III** and **IV** via nucleophilic pathway.

[2.2.3.4] Activation of Silane

Carbenes are also known to activate enthalpically strong Si–H bond for a variety of silanes [43,52]. Generally, activation of the Si–H bond of silane may proceed via two different pathways, viz., proton and hydride transfer [83]. In the proton transfer pathway, the carbene σ_{LP} interacts with one of the Si–H bonds of SiH_3Ph generating a proton and a SiH_2Ph fragment that migrates to C_C yielding the Si–H bond splitting product. The overall process proceeds via a TS exhibiting a 3c–2e interaction between the participating fragments (Figure 2.2.15).

It is clear from Figure 2.2.15 that both the TSs, **1TS$_{PT}^{Si–H}$** and **3TS$_{PT}^{Si–H}$** exhibit an elongated and polarized Si–H bond (Table 2.2.10) with the positively polarized hydrogen

interacting with the C_C (WBI = 0.551–0.561) while the SiH_2Ph fragment remains distant from the C_C (2.998–3.016 Å). Further, the TSs, **1TS$_{PT}^{Si–H}$** and **3TS$_{PT}^{Si–H}$** computes slightly larger ∠N–C_C–N bond angle from their respective parent MNHCs however, there is no appreciable change in their calculated N–C_C bond lengths (Table 2.2.10 and Figure 2.2.1).

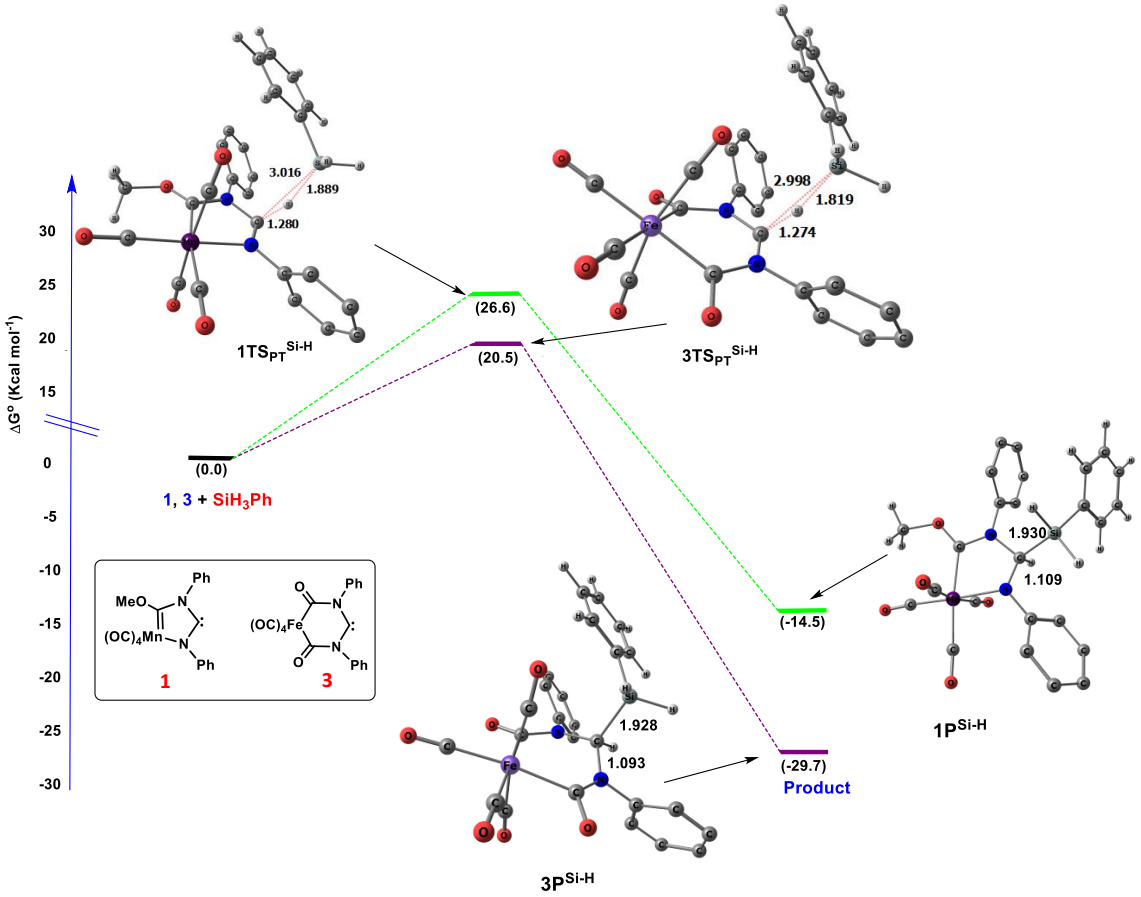

Figure 2.2.15: Energy profile diagram for the activation of Si–H bond of SiH_3Ph by **1** and **3** via proton transfer pathway at M06-D3/def2-TZVP (Toluene) level of theory. The hydrogen atoms of the phenyl rings are omitted for clarity.

The calculated activation barrier ($\Delta G°_{TS_{PT}}^{Si\text{-}H‡}$) values for **1** and **3** (Table 2.2.11) are found to be comparable to those obtained for DAC (**III**, 19.9 kcal mol^{-1}) and CAAC (**IV**, 22.7 kcal mol^{-1}) which were known to activate enthalpically strong Si–H bond for a wide range of silanes [43, 52]. The calculated reaction free energy ($\Delta G°_{Total}^{Si\text{-}H}$) values are found to be considerably exergonic (Table 2.2.11). Further, the optimized geometries of the TSs

and Si–H splitting product obtained from **III** and **IV** via proton transfer pathway is shown in Figure 2.2.16.

Table 2.2.10: Calculated (M06-D3/def2-TZVP (Toluene)) important geometrical parameters and natural charges at the silicon atom of the SiH_2Ph fragment (q_{SiH_2Ph}) and hydrogen atom ($q_H^{\delta+}$) and occupancies of the formally vacant p_π orbital at the carbene center (Occ_{P_π}) of the transition states involved in activation of the Si–H bond of SiH_3Ph by **1**, **3**, DAC (**III**) and CAAC (**IV**) via proton transfer pathway. Bond lengths, bond angles (∠N-C_C-X, X = C, N) are given in Å and in degree (°) respectively and Wiberg Bond Index (WBI) values are given within parentheses.

Molecules	$PhH_2Si^{\delta+}$–$H^{\delta-}$	C_C–SiH_2Ph	C_C–$H^{\delta+}$	C_C-X	∠N-C_C-X	q_{SiH_2Ph}	$q_H^{\delta+}$	Occ_{p_π}
IIITS_{PT}^{Si-H}	1.817	2.922	1.261	1.369/1.369	118.0	0.837	0.068	0.995
	(0.356)	(0.339)	(0.583)	(1.117)/(1.115)				
IVTS_{PT}^{Si-H}	1.861	2.983	1.281	1.325/1.506	107.7	0.706	0.095	0.825
	(0.370)	(0.365)	(0.575)	(1.323)/(0.995)				
1TS_{PT}^{Si-H}	1.889	3.016	1.280	1.301/1.411	113.2	0.659	0.096	0.951
	(0.383)	(0.276)	(0.551)	(1.461)/(1.272)				
3TS_{PT}^{Si-H}	1.819	2.998 (0.323)	1.274	1.359/1.361	123.2	0.793	0.062	0.895
	(0.379)		(0.561)	(1.148)/(1.141)				

Table 2.2.11: Calculated (M06-D3/def2-TZVP (Toluene)) activation energy barrier (kcal mol^{-1}) for proton transfer ($\Delta G°_{TS_{PT}}^{\ddagger}$) and hydride transfer ($\Delta G°_{TS_{Hy}}^{\ddagger}$) pathways, reaction free energies (kcal mol^{-1}) for the formation of the van der Waals complex ($\Delta G°_V$) and Si–H splitting product ($\Delta G°_{Total}^{Si-H}$).

Molecules	$\Delta G°_{TS_{PT}}^{\ddagger}$	$\Delta G°_V$	$\Delta G°_{TS_{Hy}}^{\ddagger}$	$\Delta G°_{Total}^{Si-H}$
III	19.9	1.4	17.1	-30.7
IV	22.7	3.4	11.3	-34.8
1	26.6	3.1	19.5	-14.5
3	20.5	2.9	17.9	-29.7

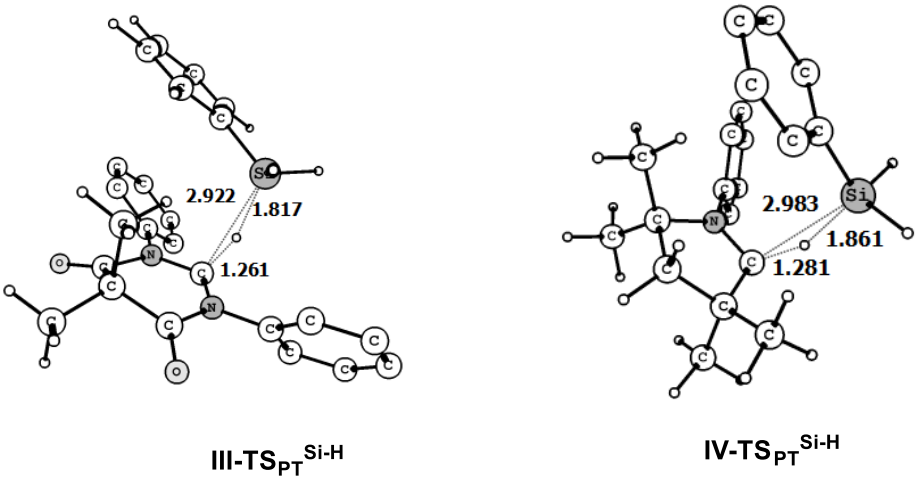

III-TS$_{PT}^{Si-H}$ IV-TS$_{PT}^{Si-H}$

(a)

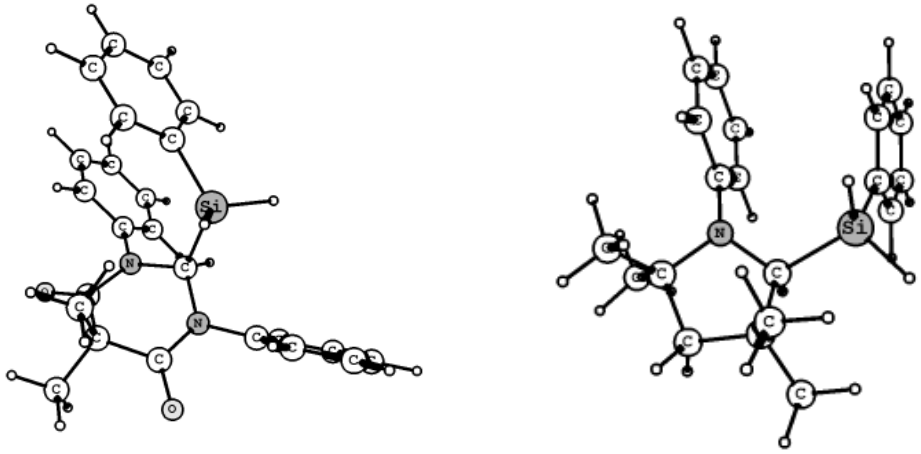

III-P^{Si-H} IV-P^{Si-H}

(b)

Figure 2.2.16: Optimized geometries (M06-D3/def2-TZVP (Toluene)) of the (a) TS (via proton transfer pathway) and (b) Si–H bond splitting product obtained for **III** and **IV**.

Unlike the proton transfer pathway which proceeds via a TS, the hydride transfer pathway proceeds via two successive steps [83]. In the first step, the σ_{LP} interact with lower lying orbital of SiH_3Ph generating van der Waals complexes $\mathbf{1_v}$ and $\mathbf{3_v}$ (Figure 2.2.17). $\mathbf{1_v}$ and $\mathbf{3_v}$ exhibit an elongated C_C–Si bond (3.146 - 3.244 Å) which were found to be within the sum of van der Waals radii of Si (2.1 Å) and C (1.7 Å) and lie at a slightly higher energy (*ca.* 2.9 – 3.1 kcal mol^{-1}) than the reactants. In the second step, $\mathbf{1_v}$ and $\mathbf{3_v}$ led to the desired

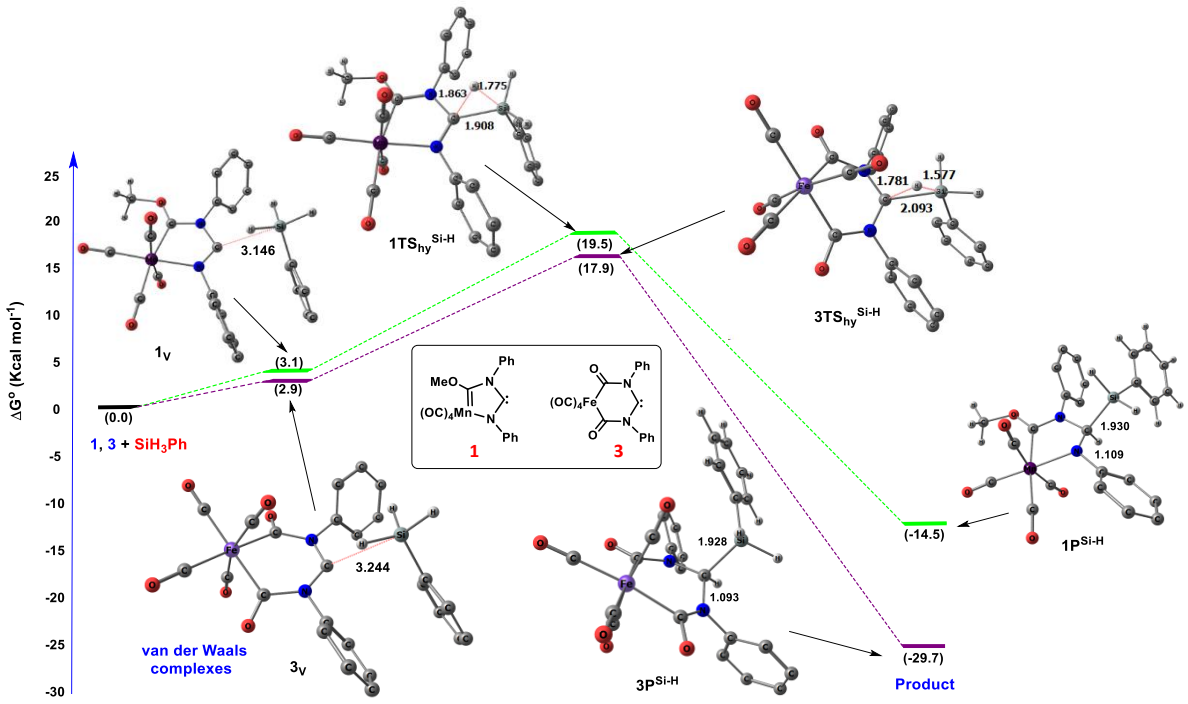

Figure 2.2.17: Energy profile diagram for the activation of Si–H bond of SiH_3Ph by **1** and **3** via hydride transfer pathway at M06-D3/def2-TZVP (Toluene) level of theory. The hydrogen atoms of the phenyl rings are omitted for clarity.

product via a TS (**1TS$_{hy}^{Si-H}$** and **3TS$_{hy}^{Si-H}$**) with activation energy barrier 19.5 and 17.9 kcal mol^{-1} respectively (Table 2.2.11). **1TS$_{hy}^{Si-H}$** and **3TS$_{hy}^{Si-H}$** exhibit an elongated and a highly polarized Si–H bond (Table 2.2.12) with the positively polarized SiH_2Ph fragments having substantial interaction with the C_C (WBI = 0.499 - 0.713) while the hydridic hydrogens ($H^{\delta-}$) reside in a bridging position between the C_C and SiH_2Ph fragment. In addition, a significant increase in the occupancies of the formally vacant p_π orbital centered at the C_C of **1TS$_{hy}^{Si-H}$** and **3TS$_{hy}^{Si-H}$** further corroborate the presence of substantial bonding interaction between the C_C and the hydridic hydrogens. Further, the TSs, **1TS$_{hy}^{Si-H}$** and **3TS$_{hy}^{Si-H}$** exhibits slightly elongated C_C-N bond lengths and also a larger ∠N-C_C-N bond angle from their respective parent MNHCs (Table 2.2.12 and Figure 2.2.1). This is followed by the migration

Table 2.2.12: Calculated (M06-D3/def2-TZVP (Toluene)) important geometrical parameters and natural charges at the silicon atom of the $SiH_2Ph^{\delta+}$ fragment ($q_{SiH_2Ph}{}^{\delta+}$) and hydridic hydrogen atom ($q_H{}^{\delta-}$) and occupancies of the formally vacant p_π orbital at the carbene center (Occ_{P_π}) of the transition states involved in activation of the Si–H bond of SiH_3Ph by **1**, **3**, DAC (**III**) and CAAC (**IV**) via hydride transfer pathway. Bond lengths, bond angles (∠N-C_c-X, X = C, N) are given in Å and in degree (°) respectively and Wiberg Bond Index (WBI) values are given within parentheses.

Molecule	$PhH_2Si^{\delta+}$–$H^{\delta-}$	C_C–$SiH_2Ph^{\delta+}$	C_C–$H^{\delta-}$	C_C-X	∠N-C_C-X	$q_{SiH_2Ph}{}^{\delta+}$	$q_H{}^{\delta-}$	Occ_{P_π}
$IIITS_{hy}^{Si-H}$	1.609	2.045	1.787	1.371/1.373	116.0	0.997	-0.091	0.735
	(0.514)	(0.551)	(0.322)	(1.121)/(1.113)				
$IVTS_{hy}^{Si-H}$	1.619	1.956	1.909	1.319/1.518	108.6	0.978	-0.150	0.737
	(0.534)	(0.645)	(0.282)	(1.327)/(0.983)				
$1TS_{hy}^{Si-H}$	1.775	1.908	1.863	1.307/1.421	111.6	1.014	-0.224	0.856
	(0.380)	(0.713)	(0.292)	(1.432)/(0.969)				
$3TS_{hy}^{Si-H}$	1.577	2.093	1.781	1.372/1.368	119.7	1.000	-0.090	0.714
	(0.550)	(0.499)	(0.307)	(1.112)/(1.122)				

of the hydridic hydrogen from the activated Si–H bond to C_c producing the Si–H bond splitting product. Furthermore, the calculated free energies of activation ($\Delta G°_{TS_{Hy}}{}^{Si-H^{\ddagger}}$) for **1**and **3** via the hydride transfer pathway are found to be somewhat comparable to DAC (**III**, 17.1 kcal mol^{-1}) but higher than that computed for CAAC (**IV**, 11.3 kcal mol^{-1}). Further, the optimized geometries of the van der Waals complexes and TSs obtained from **III** and **IV** via hydride transfer pathway is shown in Figure 2.2.18.

Thus, it may be concluded that for the MNHCs, **1** and **3** the hydride transfer pathway is found to be more favorable than the proton transfer pathway for the activation of SiH_3Ph. Also, the calculated free energies of activation for both paths are found to be comparable to those obtained for the experimentally evaluated DAC (**III**) and CAAC (**IV**) thereby indicating the possibility of activation of silane by MNHCs, **1** and **3**.

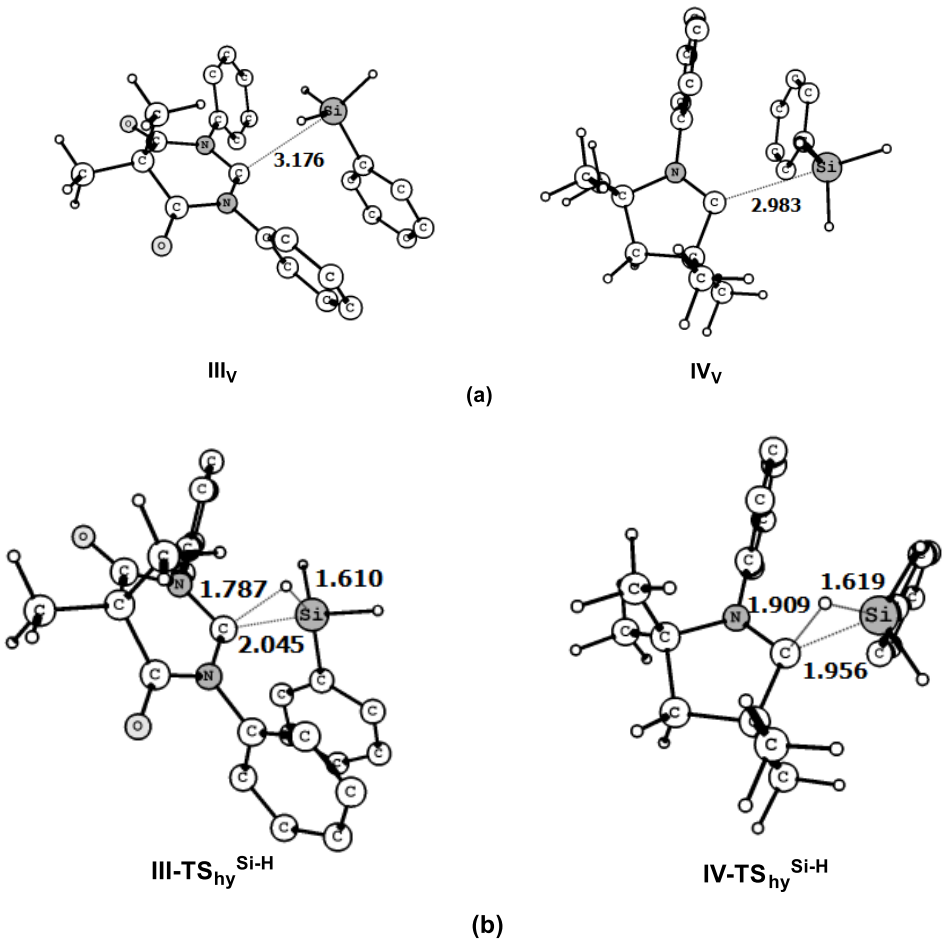

Figure 2.2.18: Optimized geometries (M06-D3/def2-TZVP (Toluene)) of the van der Waals complexes and TSs obtained from **III** and **IV** via hydride transfer pathway.

[2.2.4] Conclusions

Density functional theory calculations have been carried out to investigate the unprecedented reactivity of the computationally proposed MNHCs (**1** and **3**) towards activation of a range of small molecules. All the MNHCs have been found to have a stable singlet ground state and exhibit superior electron donating and accepting ability compared to their respective parent carbenes. Furthermore, the calculated energy barrier for the activation of a variety of enthalpically strong bonds for the MNHCs, **1** and **3** are found to be comparable to those obtained for the experimentally evaluated carbenes CAAC and DAC. In the case of silane activation, a hydride transfer pathway was found to be more favorable for the activation of Si–H bonds than a proton transfer one. We hope that the conclusions

gathered from this computational investigation will guide the experimental search for new and reactive carbenes that are capable of achieving difficult small-molecule activations.

[2.2.5] Bibliography

[1] Bertrand, G. (2002), *Carbene chemistry: from fleeting intermediates to powerful reagents*, CRC Press, New York,

[2] Igau, A., Grutzmacher, H., Baceiredo, A., and Bertrand, G. Analogous. α,α'-Bis-carbenoid, Triply Bonded Species: Synthesis of a Stable λ^3-Phosphino Carbene-λ^5-Phosphaacetylene. *Journal of the American Chemical Society*, 110(19):6463-6466, 1988.

[3] Arduengo III, A. J., Harlow, R. L., and Kline, M. A Stable Crystalline Carbene. *Journal of the American Chemical Society*, 113(1):361-363, 1991.

[4] Hopkinson, M. N., Richter, C., Schedler, M., and Glorius, F. An overview of N-heterocyclic carbenes. *Nature*, 510(7506):485-496, 2014.

[5] Nolan, S. P. The Development and Catalytic Uses of N-Heterocyclic Carbene Gold Complexes. *Accounts of Chemical Research*, 44(2):91-100, 2011.

[6] Vougioukalakis, G. C., and Grubbs, R. H. Ruthenium-Based Heterocyclic Carbene-Coordinated Olefin Metathesis Catalysts. *Chemical Reviews*, 110(3):1746-1787, 2010.

[7] Nesterov, V., Reiter, D., Bag, P., Frisch, P., Holzner, R., Porzelt, A., and Inoue, S. NHCs in Main Group Chemistry. *Chemical Reviews*, 118(19):9678-9842, 2018.

[8] Doddi, A., Peters, M., and Tamm, M. N-Heterocyclic Carbene Adducts of Main Group Elements and Their Use as Ligands in Transition Metal Chemistry. *Chemical Reviews*, 119(12): 6994-7112, 2019.

[9] Würtemberger-Pietsch, S., Radius, U., and Marder, T. B. 25 years of N-heterocyclic carbenes: activation of both main-group element–element bonds and NHCs themselves. *Dalton Transactions*, 45(14):5880-5895, 2016.

[10] Herrmann, W. A., Elison, M., Fischer, J., Köcher, C., and Artus, G. R. Metal Complexes of N-Heterocyclic Carbenes—A New Structural Principle for Catalysts in Homogeneous Catalysis. *Angewandte Chemie International Edition in English*, 34(21):2371-2374, 1995.

[11] Stauffer, S. R., Lee, S., Stambuli, J. P., Hauck, S. I., and Hartwig, J. F. High Turnover Number and Rapid, Room-Temperature Amination of Chloroarenes Using Saturated Carbene Ligands. *Organic Letters*, 2(10):1423-1426, 2000.

[12] Herrmann, W. A. N-Heterocyclic Carbenes: A New Concept in Organometallic Catalysis. *Angewandte Chemie International Edition*, 41(8):1290-1309, 2002.

[13] Diez-Gonzalez, S., Marion, N., and Nolan, S. P. N-Heterocyclic Carbenes in Late Transition Metal Catalysis. *Chemical Reviews*, 109(8):3612-3676, 2009.

[14] Enders, D., Niemeier, O., and Henseler, A. Organocatalysis by N-Heterocyclic Carbenes. *Chemical Reviews*, 107(12):5606-5655, 2007.

[15] Martin, D., Baceiredo, A., Gornitzka, H., Schoeller, W. W., and Bertrand, G. A Stable P-Heterocyclic Carbene. *Angewandte Chemie International Edition*, 44(11):1700-1703, 2005.

[16] Masuda, J. D., Martin, D., Lyon-Saunier, C., Baceiredo, A., Gornitzka, H., Donnadieu, B., and Bertrand, G. Stable P-Heterocyclic Carbenes: Scope and Limitations. *Chemistry–An Asian Journal*, 2(1):178-187, 2007.

[17] Melaimi, M., Soleilhavoup, M., and Bertrand, G. Stable Cyclic Carbenes and Related Species beyond Diaminocarbenes. *Angewandte Chemie International Edition*, 49(47):8810-8849, 2010.

[18] Ruiz, J., and Perandones, B. F. Metal-induced tautomerization of oxazole and thiazole molecules to heterocyclic carbenes. *Chemical Communications*, (19):2741-2743, 2009.

[19] Vougioukalakis, G. C., and Grubbs, R. H. Synthesis and Activity of Ruthenium Olefin Metathesis Catalysts Coordinated with Thiazol-2-ylidene Ligands. *Journal of the American Chemical Society*, 130(7):2234-2245, 2008.

[20] Raubenheimer, H. G., and Cronje, S. Carbene complexes derived from lithiated heterocycles, mainly azoles, by transmetallation. *Journal of Organometallic Chemistry*, 617-618:170-181, 2001.

[21] Raubenheimer, H. G., Stander, Y., Marais, E. K., Thompson, C., Kruger, G. J., Cronje, S., and Deetlefs, M. Group 6 carbene complexes derived from lithiated azoles and the crystal structure of a molybdenum thiazolinylidene complex. *Journal of Organometallic Chemistry*, 590(2):158-168, 1999.

[22] Chien, S. W., Yen, S. K., and Hor, T. A. N, S-heterocyclic carbene complexes. *Australian Journal of Chemistry*, 63(5):727-741, 2010.

[23] Kausamo, A., Tuononen, H. M., Krahulic, K. E., and Roesler, R. *N*-Heterocyclic Carbenes with Inorganic Backbones: Electronic Structures and Ligand Properties. *Inorganic Chemistry*, 47(3):1145-1154, 2008.

[24] Krahulic, K. E., Tuononen, H. M., Parvez, M., and Roesler, R. Isolation of Free Phenylide-like Carbanions with N-Heterocyclic Carbene Frameworks. *Journal of the American Chemical Society*, 131(16):5858-5865, 2009.

[25] Krahulic, K. E., Enright, G. D., Parvez, M., and Roesler, R. A Stable N-heterocyclic Carbene with a Diboron Backbone. *Journal of the American Chemical Society*, 127(12):4142-4143, 2005.

[26] Präsang, C., Donnadieu, B., and Bertrand, G. Stable Planar Six-π-Electron Six-Membered N-Heterocyclic Carbenes with Tunable Electronic Properties. *Journal of the American Chemical Society*, 127(29):10182-10183, 2005.

[27] Despagnet-Ayoub, E., and Grubbs, R. H. A Stable Four-Membered N-Heterocyclic Carbene. *Journal of the American Chemical Society*, 126(33):10198-10199, 2004.

[28] Forster, T. D., Krahulic, K. E., Tuononen, H. M., McDonald, R., Parvez, M., and Roesler, R. A σ-Donor with a Planar Six-π-Electron $B_2N_2C_2$ Framework: Anionic N-Heterocyclic Carbene or Heterocyclic Terphenyl Anion?. *Angewandte Chemie International Edition*, 45(38):6356-6359, 2006.

[29] Gründemann, S., Kovacevic, A., Albrecht, M., Robert, J. W. F., and Crabtree, H. Abnormal binding in a carbene complex formed from an imidazolium salt and a metal hydride complex. *Chemical Communications*, (21):2274-2275, 2001.

[30] Gruendemann, S., Kovacevic, A., Albrecht, M., Faller, J. W., and Crabtree, R. H. Abnormal Ligand Binding and Reversible Ring Hydrogenation in the Reaction of Imidazolium Salts with $IrH_5(PPh_3)_2$. *Journal of the American Chemical Society*, 124(35):10473-10481, 2002.

[31] Mathew, P., Neels, A., and Albrecht, M. 1,2,3-Triazolylidenes as Versatile Abnormal Carbene Ligands for Late Transition Metals. *Journal of the American Chemical Society*, 130(41):13534-13535, 2008.

[32] Guisado-Barrios, G., Bouffard, J., Donnadieu, B., and Bertrand, G. Crystalline 1H-1,2, 3-Triazol-5-ylidenes: New Stable Mesoionic Carbenes (MICs). *Angewandte Chemie International Edition*, 49(28):4759-4762, 2010.

[33] Denk, M. K., Gupta, S., and Lough, A. J. Aromatic Phosphenium Cations. *European Journal of Inorganic Chemistry*, 1999(1):41-49, 1999.

[34] Gudat, D. Cation Stabilities, Electrophilicities, and "Carbene Analogue" Character of Low Coordinate Phosphorus Cations. *European Journal of Inorganic Chemistry*, 1998(8):1087-1094, 1998.

[35] Gudat, D., Haghverdi, A., Hupfer, H., and Nieger, M. Stability and Electrophilicity of Phosphorus Analogues of Arduengo Carbenes—An Experimental and Computational Study. *Chemistry–A European Journal*, 6(18):3414-3425, 2000.

[36] Denk, M., Lennon, R., Hayashi, R., West, R., Belyakov, A. V., Verne, H. P., Haaland, A., Wagner M., and Metzler N. Synthesis and Structure of a Stable Silylene. *Journal of the American Chemical Society*, 116(6):2691-2692, 1994.

[37] Haaf, M., Schmedake, T. A., and West, R. Stable Silylenes. *Accounts of Chemical Research*, 33(10):704-714, 2000.

[38] Lavallo, V., Canac, Y., Präsang, C., Donnadieu, B., and Bertrand, G. Stable Cyclic (Alkyl)(Amino)Carbenes as Rigid or Flexible, Bulky, Electron-Rich Ligands for Transition-Metal Catalysts: A Quaternary Carbon Atom Makes the Difference. *Angewandte Chemie International Edition*, 44(35):5705-5709, 2005.

[39] Lavallo, V., Canac, Y., DeHope, A., Donnadieu, B., and Bertrand, G. A Rigid Cyclic (Alkyl)(amino)carbene Ligand Leads to Isolation of Low-Coordinate Transition-Metal Complexes. *Angewandte Chemie International Edition*, 44(44):7236-7239, 2005.

[40] Frey, G. D., Lavallo, V., Donnadieu, B., Schoeller, W. W., and Bertrand, G. Facile Splitting of Hydrogen and Ammonia by Nucleophilic Activation at a Single Carbon Center. *Science*, 316(5823):439-441, 2007.

[41] Lavallo, V., Canac, Y., Donnadieu, B., Schoeller, W. W., and Bertrand, G. CO Fixation to Stable Acyclic and Cyclic Alkyl Amino Carbenes: Stable Amino Ketenes with a Small HOMO–LUMO Gap. *Angewandte Chemie International Edition*, 45(21):3488-3491, 2006.

[42] Masuda, J. D., Schoeller, W. W., Donnadieu, B., and Bertrand, G. Carbene Activation of P_4 and Subsequent Derivatization. *Angewandte Chemie International Edition*, 46(37):7052-7055, 2007.

[43] Frey, G. D., Masuda, J. D., Donnadieu, B., and Bertrand, G. Activation of Si–H, B–H, and P–H Bonds at a Single Nonmetal Center. *Angewandte Chemie International Edition*, 122(49):9634-9637, 2010.

[44] Paul, U. S., and Radius, U. Ligand versus Complex: C−F and C−H Bond Activation of Polyfluoroaromatics at a Cyclic (Alkyl)(Amino) Carbene. *Chemistry–A European Journal*, 23(16):3993-4009, 2017.

[45] Turner, Z. R. Chemically Non-Innocent Cyclic (Alkyl)(Amino) Carbenes: Ligand Rearrangement, C−H and C−F Bond Activation. *Chemistry–A European Journal*, 22(32):11461-11468, 2016.

[46] Styra, S., Melaimi, M., Moore, C. E., Rheingold, A. L., Augenstein, T., Breher, F., and Bertrand, G. Crystalline Cyclic (Alkyl)(amino) Carbene-tetrafluoropyridyl Radical. *Chemistry–A European Journal*, 21(23):8441-8446, 2015.

[47] Martin, D., Soleilhavoup, M., and Bertrand, G. Stable singlet carbenes as mimics for transition metal centers. *Chemical Science*, 2(3):389-399, 2011.

[48] Melaimi, M., Jazzar, R., Soleilhavoup, M., and Bertrand, G. Cyclic (Alkyl)(amino)carbenes (CAACs): Recent Developments. *Angewandte Chemie International Edition*, 56(34):10046-10068, 2017.

[49] Paul, U. S., and Radius, U. What Wanzlick Did Not Dare To Dream: Cyclic (Alkyl)(amino) carbenes (CAACs) as New Key Players in Transition-Metal Chemistry. *European Journal of Inorganic Chemistry*, 2017(28):3362-3375, 2017.

[50] Soleilhavoup, M., and Bertrand, G. Cyclic (lkyl)(amino) carbenes (CAACs): Stable Carbenes on the Rise. *Accounts of Chemical Research*, 48(2):256-266, 2015.

[51] Hudnall, T. W., and Bielawski, C. W. An *N, N′*-Diamidocarbene: Studies in C−H Insertion, Reversible Carbonylation, and Transition-Metal Coordination Chemistry. *Journal of the American Chemical Society*, 131(44):16039-16041, 2009.

[52] Lastovickova, D. N., Moerdyk, J. P., Kelley, A. R., and Bielawski, C. W. Assessing the reactivity of the N, N′-diamidocarbenes toward compounds containing early p-block elements. *Journal of Physical Organic Chemistry*, 28(2):75-78, 2015.

[53] Hudnall, T. W., Moerdyk, J. P., and Bielawski, C. W. Ammonia N–H activation by a N, N′-diamidocarbene. *Chemical Communications*, 46(24):4288-4290, 2010.

[54] Moerdyk, J. P., and Bielawski, C. W. Reductive generation of stable, five-membered N, N′-diamidocarbenes. *Chemical Communications*, 50(35):4551-4553, 2014.

[55] Moerdyk, J. P., Blake, G. A., Chase, D. T., and Bielawski, C. W. Elucidation of Carbene Ambiphilicity Leading to the Discovery of Reversible Ammonia Activation. *Journal of the American Chemical Society*, 135(50):18798-18801, 2013.

[56] Moerdyk, J. P., and Bielawski, C. W. N, N′-Diamidocarbenes Facilitate Selective C−H Insertions and Transfer Hydrogenations. *Chemistry–A European Journal*, 19(44):14773-14776, 2013.

[57] Chase, D. T., Moerdyk, J. P., and Bielawski, C. W. Exploring the Chemistry of *N, N′*-Diamidocarbenes with Organophosphorus Compounds. *Organic Letters*, 16(3), 812-815, 2014.

[58] Ruiz, J., García, L., Mejuto, C., Vivanco, M., Díaz, M. R., and García-Granda, S. Strong electron-donating metalla-N-heterocyclic carbenes. *Chemical Communications*, 50(17):2129-2132, 2014.

[59] Ruiz, J., García, L., Vivanco, M., Berros, Á., and Van der Maelen, J. F. Generating and Trapping Metalla-N-Heterocyclic Carbenes. *Angewandte Chemie International Edition*, 127(14):4286-4290, 2015.

[60] Beaumier, E. P., Gordon, C. P., Harkins, R. P., McGreal, M. E., Wen, X., Copéret, C., Goodpaster, J. D., and Tonks, I. A. $Cp_2Ti(\kappa^2\text{-}^t BuNCN^t Bu)$: A Complex with an Unusual κ^2 Coordination Mode of a Heterocumulene Featuring a Free Carbene. *Journal of the American Chemical Society*, 142(17):8006-8018, 2020.

[61] Boehme, C., and Frenking, G. Electronic Structure of Stable Carbenes, Silylenes, and Germylenes. *Journal of the American Chemical Society*, 118(8):2039-2046, 1996.

[62] Tukov, A. A., Normand, A. T., and Nechaev, M. S. N-heterocyclic carbenes bearing two, one and no nitrogen atoms at the ylidene carbon: insight from theoretical calculations. *Dalton Transactions*, (35):7015-7028, 2009.

[63] Bazinet, P., Yap, G. P., and Richeson, D. S. Constructing a Stable Carbene with a Novel Topology and Electronic Framework. *Journal of the American Chemical Society*, 125(44):13314-13315, 2003.

[64] Nair, V., Bindu, S., and Sreekumar, V. N-Heterocyclic Carbenes: Reagents, Not Just Ligands!. *Angewandte Chemie International Edition*, 43(39):5130-5135, 2004.

[65] Phukan, A. K., Guha, A. K., Sarmah, S., and Dewhurst, R. D. Electronic and Ligand Properties of Annelated Normal and Abnormal (Mesoionic) *N*-heterocyclic Carbenes: A Theoretical Study. *The Journal of Organic Chemistry*, 78(21):11032-11039, 2013.

[66] Borthakur, B., Rahman, T., and Phukan, A. K. Tuning the Electronic and Ligand Properties of Remote Carbenes: A Theoretical Study. *The Journal of Organic Chemistry*, 79(22):10801-10810, 2014.

[67] Takahashi, S., Bellan, E., Baceiredo, A., Saffon-Merceron, N., Massou, S., Nakata, N., Hashizume, D., Branchadell, V., and Kato, T. A Stable N-Hetero-*Rh*-Metallacyclic Silylene. *Angewandte Chemie International Edition*, 131(30):10416-10420, 2019.

[68] Zhao, Y., and Truhlar, D. G. The M06 suite of density functionals for main group thermochemistry, thermochemical kinetics, noncovalent interactions, excited states, and transition elements: two new functionals and systematic testing of four M06-class functionals and 12 other functionals. *Theoretical Chemistry Accounts*, 120(1):215-241, 2008.

[69] Weigend, F., and Ahlrichs, R. Balanced basis sets of split valence, triple zeta valence and quadruple zeta valence quality for H to Rn: Design and assessment of accuracy. *Physical Chemistry Chemical Physics*, 7(18):3297-3305, 2005.

[70] Weigend, F. Accurate Coulomb-fitting basis sets for H to Rn. *Physical Chemistry Chemical Physics*, 8(9):1057-1065, 2006.

[71] Grimme, S., Antony, J., Ehrlich, S., and Krieg, H. A consistent and accurate ab initio parametrization of density functional dispersion correction (DFT-D) for the 94 elements H-Pu. *The Journal of Chemical Physics*, 132(15):154104, 2010.

[72] Cossi, M., Scalmani, G., Rega, N., and Barone, V. New developments in the polarizable continuum model for quantum mechanical and classical calculations on molecules in solution. *The Journal of Chemical Physics*, 117(1):43-54, 2002.

[73] Glendening, E. D., Reed, A. E., Carpenter, J. E., and Weinhold, F. NBO Program, version 3.1; University of Wisconsin: Madison, WI, 1988

[74] Reed, A. E., Curtiss, L. A., and Weinhold, F. Intermolecular Interactions from a Natural Bond Orbital, Donor-Acceptor Viewpoint. *Chemical Reviews*, 88(6):899-926, 1988.

[75] Frisch, M. J., Trucks, G. W., Schlegel, H. B., Scuseria, G. E., Robb, M. A., Cheeseman, J. R., Montgomery, J. A., Jr., Vreven, T., Kudin, K. N., Burant, J. C., Millam, J. M., Iyengar, S. S., Tomasi, J., Barone, V., Mennucci, B., Cossi, M., Scalmani, G., Rega, N., Petersson, G. A., Nakatsuji, H., Hada, M., Ehara, M., Toyota, K., Fukuda, R., Hasegawa, J., Ishida, M., Nakajima, T., Honda, Y., Kitao, O., Nakai, H., Klene, M., Li, X., Knox, J. E., Hratchian, H. P., Cross, J. B., Bakken, V., Adamo, C., Jaramillo, J., Gomperts, R., Stratmann, R. E., Yazyev, O., Austin, A. J., Cammi, R., Pomelli, C., Ochterski, J. W., Ayala, P. Y., Morokuma, K., Voth, G. A., Salvador, P. J., Dannenberg, J., Zakrzewski, V. G., Dapprich, S., Daniels, A. D., Strain, M. C., Farkas, O., Malick, D. K., Rabuck, A. D., Raghavachari, K., Foresman, J. B., Ortiz, J. V., Cui, Q., Baboul, A. G., Clifford, S., Cioslowski, J., Stefanov, B. B., Liu, G., Liashenko, A., Piskorz, P., Komaromi, I., Martin, R. L., Fox, D. J., Keith, T., Al- Laham, M. A., Peng, C. Y., Nanayakkara, A., Challacombe, M., Gill, P. M. W., Johnson, B., Chen, W., Wong, M. W., Gonzalez, C., and Pople, J. A. *Gaussian 03, Revision D.02*; Gaussian, Inc., Pittsburgh, PA, 2003.

[76] Bourissou, D., Guerret, O., Gabbaï, F. P., and Bertrand, G. Stable Carbenes. *Chemical Reviews*, 100(1):39-92, 2000.

[77] Gronert, S., Keeffe, J. R., and More O'Ferrall, R. A. Stabilities of Carbenes: Independent Measures for Singlets and Triplets. *Journal of the American Chemical Society*, 133(10):3381-3389, 2011.

[78] Munz, D. Pushing Electrons–Which Carbene Ligand for Which Application?. *Organometallics*, 37(3):275-289, 2018.

[79] Bharadwaz, P., Chetia, P., and Phukan, A. K. Electronic and Ligand Properties of Skeletally Substituted Cyclic (Alkyl)(Amino) Carbenes (CAACs) and Their Reactivity Towards Small Molecule Activation: A Theoretical Study. *Chemistry–A European Journal*, 23(41):9926-9936, 2017.

[80] Siemeling, U., Färber, C., Bruhn, C., Leibold, M., Selent, D., Baumann, W., Hopffgarten, M. V., Goedecke, C., and Frenking, G. *N*-heterocyclic carbenes which readily add ammonia, carbon monoxide and other small molecules. *Chemical Science*, 1(6):697-704, 2010.

[81] van der Vlugt, J. I. Advances in selective activation and application of ammonia in homogeneous catalysis. *Chemical Society Reviews*, 39(6):2302-2322, 2010.

[82] Moerdyk, J. P., Schilter, D., and Bielawski, C. W. *N*, *N*′-Diamidocarbenes: Isolable Divalent Carbons with Bona Fide Carbene Reactivity. *Accounts of Chemical Research*, 49(8):1458-1468, 2016.

[83] Bharadwaz, P., Dewhurst, R. D., and Phukan, A. K. Metal-Free Activation of Enthalpically Strong Bonds: Unraveling the Potential of Hitherto Unexplored Singlet Carbenes. *Advanced Synthesis & Catalysis*, 360(23):4543-4561, 2018.